This is a non-peer reviewed preprint submitted to EarthArxiv.

Please feel free to contact any of the authors; we welcome feedback

The influence of a slope break on turbidite deposits: an experimental investigation

Pohl, F.[a]*, Eggenhuisen, J.T.[a], Cartigny, M.J.B.[b], Tilston, M.[a], de Leeuw, J.[a], Hermidas, N.[c]

[a] Faculty of Geosciences, Utrecht University, P.O. box 80021, 3508 TA Utrecht, The Netherlands
[b] Departments of Geography, Durham University, Lower Mountjoy South Road, DH1 3LE Durham, UK
[c] Faculty of Civil Engineering and Geosciences, TU Delft, P.O. box 5048, 2600 GA Delft, The Netherlands

* Corresponding author: florian.pohl63@gmail.com

Abstract

Bypassing turbidity currents travel downslope while depositing only a minor part of their suspended sediment load. Along the way, they may encounter a slope break (i.e. an abrupt decrease in slope angle) that initiates the deposition of sediment. Depending on their proximal initiation point, these turbiditic deposits in slope-break systems can form potential reservoirs for hydrocarbons. The present experimental study establishes the resulting turbidite deposits as a function of the geometry in a slope-break system. Shields-scaled turbidity currents were released into a flume tank containing an upper and a lower slope reach, which were separated by a slope break. Results show that the depositional pattern in a slope-break system is controlled by the steepness of the upper and lower slope, rather than the severity of the slope break. The steepness of the upper slope controls the initiation point of sediment deposition, while the lower slope controls depositional thickness. Subsequently, Shields scaling is used to relate our experimental flows with natural turbidity currents and the results of numerical models. These results demonstrate that it is possible to predict the depositional patterns of slope-break systems based on the steepness of the incoming slope. Such prediction improves the risk estimation of potential hydrocarbon reservoirs in slope-break systems.

1. Introduction

Turbidity currents are subaqueous currents of sediment-laden water that move downslope as a result of the density difference between the flow and the overlying ambient water; this represent one of the main mechanisms for transporting sediment into the deep oceans (Mutti et al., 2009; Talling et al., 2015). Turbidity currents form submarine channels, which allow the currents to bypass their sediment down the continental slope and onto the deep-marine abyssal plain (Daly, 1936; Maier et al., 2011; Stevenson et al., 2015). On their downflow trajectory, turbidity currents may encounter a slope break, which is marked by an abrupt decrease in the ocean-floor gradient.

Slope breaks tend to occur in ponded basins, on stepped slopes (Brooks et al., 2018; Jobe et al., 2017; Prather, 2003; Prather et al., 2012a, 2012b), or at the base of steep active continental margins (Bourget et al., 2011; Lee et al., 2002). On the more gently dipping sea floor, turbidity currents usually switch from bypass to depositional conditions, forming sediment bodies (Amy et al., 2000; Carvajal and Steel, 2006; Lee et al., 2004; Mutti and Normark, 1991, 1987; Prélat et al., 2010; Talling et al., 2007; Wynn et al., 2000). The morphology of these deposits is controlled by the turbidity current dynamics, which are impacted by the slope break.

Sediment deposits in slope-break systems can serve as potential reservoirs for hydrocarbons (Pettingill, 2004; Weimer and Slatt, 2004; Zou et al., 2015). The likelihood of forming a sealed reservoir depends on the proximal termination point of the sediment bodies, like those seen in the Buzzard Field (Doré and Robbins, 2005; Ray et al., 2010). The location of the point where the current transitions from bypass to depositional conditions is here termed up-dip pinch-out (UDPO). If the UDPO is located upstream of the slope break, the basin floor sediments are connected to slope sediments, creating up-dip-migration pathways for hydrocarbons. In contrast, an UDPO located downstream of the slope break will result in basin floor sediments that are detached from the slope sediments, forming a stratigraphic trap and making upslope leakage of hydrocarbons less likely. Hence, the controlling factor on the UDPO is of major interest for the development of reservoir plays in slope-break systems.

Herein we present flume tank experiments designed to investigate the impact of a slope-break geometry on the location of the UDPO, and the thickness distribution of the resulting deposits. Numerous experimental studies have noted the response of flow dynamics to a slope break (Garcia and Parker, 1989; Garcia, 1993, 1994, Gray et al., 2005, 2006; Islam and Imran, 2010; Mulder and Alexander, 2001). However, these studies used continuously depletive currents (*sensu* Kneller and Branney, 1995), where deposition was initiated immediately after entering the experimental setup, even when the initial slope was steep. Such depletive conditions make it difficult to compare their depositional signatures with natural systems (e.g. Talling et al., 2012). For the present experimental study, we used Shields scaling (sensu de Leeuw et al., 2016), to generate turbidity currents that were able to ensure bypass conditions on the steepest of our experimental slopes, and transition to depositional conditions on more gentle experimental slopes. Furthermore, all previous slope-break studies used horizontal basin floors; while this condition may represent the condition for lobe development on very gently dipping surfaces ($<< 1°$), it neglects systems with steeper basin floors (e.g. stepped slopes). The

experiments presented herein were the first slope-break experiments with a non-horizontal lower slope, allowing the link to natural slope-break systems with dipping lower slopes. The research questions of this paper are: 1) What are the geometric controls on the location of the UDPO? 2) What are the geometric controls on the deposit thickness downstream of the slope break? 3) How do our experiments scale to natural turbidite systems? 4) How can the findings of the present paper be applied to natural slope-break systems?

2. Methods

The experimental setup consisted of a flume tank with a floor that was divided into an upper slope and a lower slope segment, connected by a slope break (Fig. 1). The dipping angle of both the upper and lower slopes could be adjusted independently from one another. Forty-five different combinations of upper and lower slope configurations were teste to investigate the resulting depositional morphology (Fig. 2).

To investigate the scaling of the experiments with respect to natural turbidite systems, we use the bypass-slope criterion. The bypass-slope criterion will be here referred to as the most gently dipping slope angle at which a turbidity current with a given flow thickness, sediment concentration, and grain size is still bypassing its suspended load. Following Stevenson et al. (2015), we refer to a bypassing turbidity current as a flow that keeps its entire sediment load in suspension or traction, resulting in no deposition by that flow at the point of measurement (i.e. in the flume tank). The scaling procedure require knowledge of both flow thickness and density measurements; the former was determined by measuring the velocity structure with an Ultrasonic Doppler Velocimetry Probe (UVP), and the latter was measured by particle siphoning at multiple points above the bed.

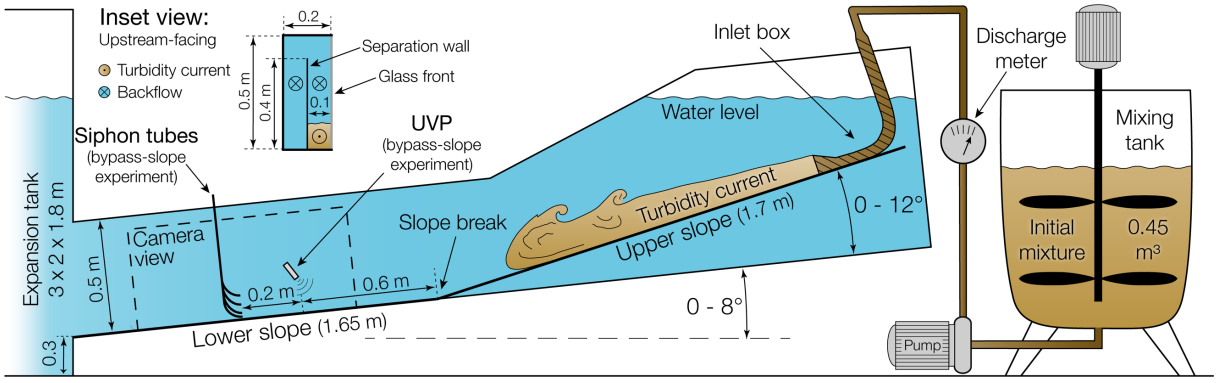

Fig. 1. Sketch of the experimental setup. The dipping angle of the upper slope were varied from 0 to 12° and the angle of the lower slope from 0 to 8° (both angles with respect to the horizontal). Inset view shows the separation of the flume tank into two channels; one was used for the turbidity current, while the second one provides additional space for the backflow. UVP: Ultrasonic Doppler Velocimetry Probe.

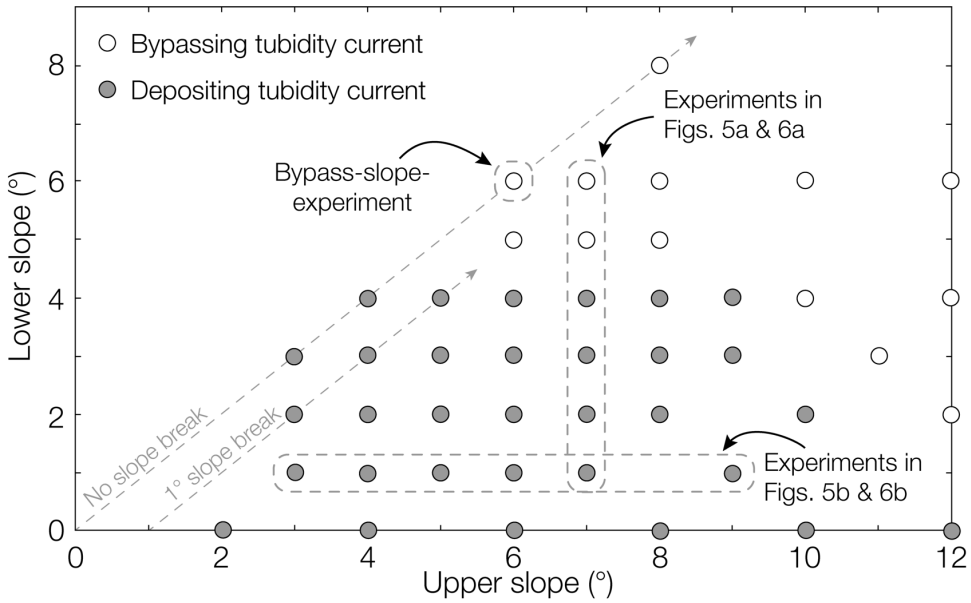

Fig. 2. Slope-break systems which were used in this study. A total of 45 different combinations of upper and lower slope angles were tested. The dipping angels of the lower and upper slope are with respect to the horizontal. The slope break is the angle between the upper and the lower slope.

2.1. Scaling

Shields scaling is used to scale a flow to specific bed roughness and sediment transport regimes. While this approach has been used previously (de Leeuw et al., 2018a, 2018b, 2016; Hermidas et al., 2018), there is no rigorous explanation of the scaling procedure in the literature. Given the significance of this approach for particle-laden flows, the following provides a detailed procedure for determining and applying the Shields scaling.

Shields scaling is based on two scaling parameters, the Reynolds particle number and the Shields parameter, which are both kept close to values encountered in natural systems. The Reynolds particle number Re_p is a function of the ratio of the grain size to the thickness of the viscous sublayer, and controls the hydraulic conditions of the flow:

$$Re_p = \frac{u_* d_b}{\nu}, \tag{1}$$

Where u_* is the shear velocity, d_b the grain size of the sediment of the bed, and ν the kinematic viscosity (we used ν of clear water at 20°C; $1*10^{-6}$ m²/s). The value Re_p extends from hydraulically smooth ($Re_p < 5$), to transitionally ($5 < Re_p < 16$), to rough ($Re_p > 16$) (Garcia, 2008). In the hydraulically-smooth regime, the particles are completely enveloped by the viscous sublayer and particle motion is driven by viscous shear stress. In a hydraulically-rough regime, the particles protrude through the viscous sublayer and are exposed to turbulent stresses. Measurements on natural turbidity currents in submarine canyons revealed a Re_p in the transitionally regime (Azpiroz-Zabala et al., 2017; Xu, 2010; Xu et al., 2014). To make

comparisons with the depositional morphology of natural systems, the experiments should be within the same hydraulic regime, which is the justification for shields scaling. Previous work using our experimental setup have reported shear velocities of ~0.07 m/s (Cartigny et al., 2014). Knowing this, the Re_p can be altered by varying d_b (i.e. the grain size used for the flume tank floor), which was set to a fine grain size (d_{10} = 35 µm, d_{50} = 133 µm, d_{90} = 214 µm; supplementary material Fig. S1) to reach Re_p values of ~7 comparable to natural systems.

The Shields parameter θ is the ratio between the shear stress and the gravity force acting on particles (Shields, 1936):

$$\theta = \frac{\rho_t u_*^2}{(\rho_s - \rho_w) g d_t}, \tag{2}$$

Where ρ_t is the density of the turbidity current, ρ_s the density of the suspended sediment (2650 kg/m³), ρ_w the density of the fluid (1000 kg/m³), d_t the grain size of the suspended sediment, and g the gravitational acceleration (9.81 m/s²). The shear velocity u_* can be defined as (Kneller, 2003):

$$u_* = \sqrt{\left(1 - \frac{\rho_w}{\rho_t}\right) g h S}. \tag{3}$$

The thickness of the flow is h and S is the tangent of the slope on which the flow moves. The density of the turbidity current ρ_t is:

$$\rho_t = (\rho_s - \rho_w) C + \rho_w, \tag{4}$$

with C as the sediment concentration. Combining equations 2, 3 and 4 results in the Shields parameter θ in a turbidity current:

$$\theta = \frac{ChS}{d_t}. \tag{5}$$

Studies on natural flows report θ-values of 1 – 10 (Azpiroz-Zabala et al., 2017; Xu, 2010; Xu et al., 2014). To meet these values in the experiments, the sediment concentration, the slope gradient, and the grain size of the suspended sediment were adjusted. We required turbidity currents with a flow thickness of ~0.1 m, flowing on slopes of between 2 – 12°, in order to be able to generate a variety of different slope-break system geometries in the available flume. The grain size of the suspended sediment d_t was already determined by the Reynolds particle number as d_b. Therefore, we set the initial sediment concentration C for the modeled turbidity currents at 17 %vol to meet the required θ-values of 1 – 10. Recent measurements from natural turbidity currents suggest high basal sediment concentrations (i.e. >> 10 %vol; Paull et al. 2018) and, therefore, are likely governed by the same processes (e.g. hindered settling), as the modeled turbidity currents.

2.2. Flume tank setup and experimental procedure

Experiments were conducted in a flume tank with the dimensions of 4 m x 0.5 m x 0.22 m (length x height x width) that included a variable slope break (Fig. 1). The turbidity currents exited the flume through a free over-fall into an expansion tank (3 m x 2 m x 1.8 m, with a floor 0.3 m lower than the flume tank floor). The currents could expand freely in the expansion tank and produced a weak reflection wave which was too slow to travel back into the experimental setup while the experiment was running. The flume and expansion tank were filled with fresh water. Sediment with an identical grain size to the sediment used in the turbidity currents was glued to the flume floor to create a rough, non-erodible surface (d_{10} = 35 µm, d_{50} = 133 µm, d_{90} = 214 µm). A longitudinally oriented separation wall subdivided the flume tank into two, 0.1m wide channels (see inset view in Fig. 1) to minimize the effect of backflow from the expansion tank into the flume during the experiments. A cantilevered false-floor was installed to adjust the bed slope on the upper and lower slope segments of the flume (Fig. 1). The steepness of the upper slope was varied between 2 and 12°, and the steepness of the lower slope between 0 and 8° (both angles with respect to the horizontal). This resulted in a total of 10 unique slope-break angles and 45 unique combinations of the upper and lower slope conditions (Fig. 2).

A mixture of sediment and fresh water with a total volume of 0.45 m³ was prepared in a mixing tank. The grain size of the sediment (d_{10} = 35 µm, d_{50} = 133 µm, d_{90} = 214 µm) was measured with a laser particle sizer (Malvern Mastersizer 2000; supplementary material Fig. S1). The density of the sediment was 2,650 kg/m³. As per the Shields scaling calculations, the sediment concentration in the mixture was set to 17 %vol, or a bulk density of 1,280 kg/m³, for each experimental flow. The mixture was pumped into the flume tank through a 4 m long pipe (pipe diameter = 0.06 m) with a radial-flow pump and monitored by a discharge meter (Krohne Optiflux 2300). The discharge was set to 12.5 ± 0.7 m³/h, resulting in a mean flow velocity of 0.81 ± 0.04 m/s at the inlet box. The duration of an experiment was ca. 100 s. Video analysis showed that the tails of all the experimental currents were accompanied by the deposition of a 7 – 10 mm thick layer of sediment over the entire length of the flume, which is hereafter called the tail deposit.

2.3. Acquisition of the depositional pattern

The thickness of the deposits was manually measured through the side-wall at longitudinal intervals of 0.05 m prior to draining the flume. In all non-bypassing runs, depositional thickness decreased rapidly over the final ~0.35 m of the flume (Fig. 3a). This rapid thinning of the deposit was an artifact of the transition from the flume into the expansion tank. Consequently, the last 0.5 m of the depositional profiles are omitted from the analysis (Fig. 3b).

The point where depositional thickness initially exceeded 10 mm is defined as the UDPO; the value of 10 mm was chosen to account for the tail deposits (cf. Fig. 3b), and therefore the origins of the UDPO are associated with the head and body of the currents. The thickness of the deposits increased from the UDPO along downstream direction. The rate of thickness increase is here referred to as the Deposit-Thickness-Increase (DTI). The DTI was calculated by taking the

slope of a local linear regression that was applied to the depositional profile. The range of the fitting function was from the location of the UDPO to 2.85 m downstream of the inlet box (Fig. 3b).

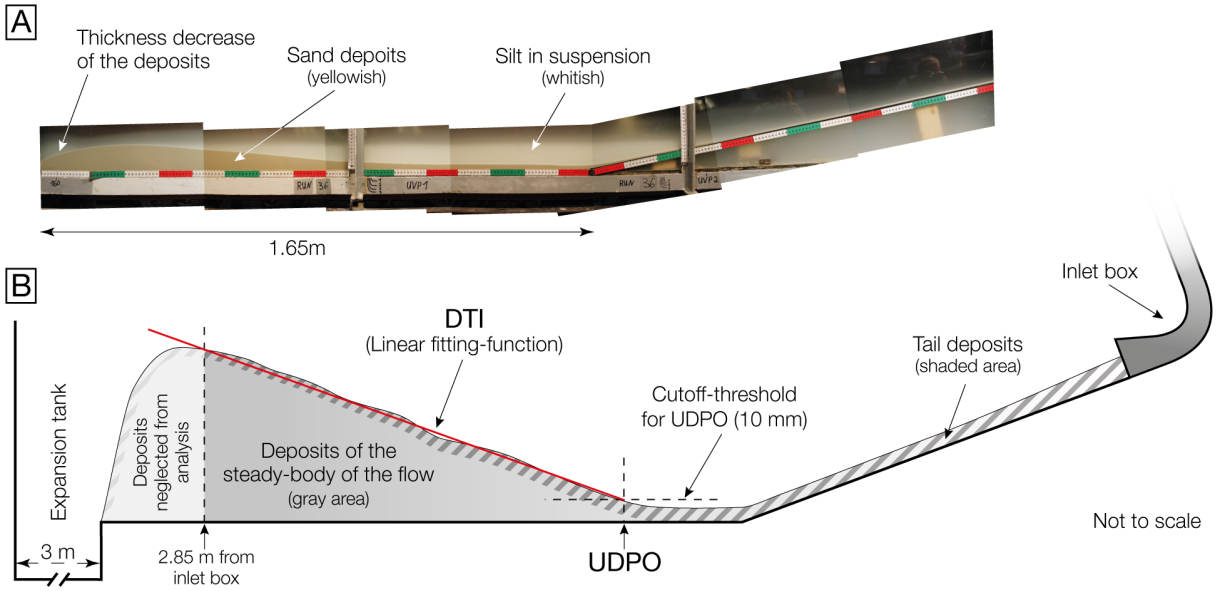

Fig. 3. (a) Photograph of the deposits of taken shortly after the end of an experiment. At the time the picture was taken, the silt fraction of the sediment was still in suspension. (b) Sketch illustrating the methods applied to analyze and parameterize the deposit profiles.

2.4. Data collection in the bypass-slope experiment

Experimentally the bypass-slope criterion was determined to be 6° for the modeled turbidity currents. For the scaling of the bypass-slope criterion to natural systems, flow thickness (h), sediment concentration (C), and grain size (d_t) of the modeled turbidity currents are required. These parameters were measured in an experimental setup with a continuous slope angle of 6°, which is here referred to as the bypass-slope experiment (cf. Fig. 2).

The flow thickness in the bypass-slope experiment was calculated from a velocity profile measurement located 2.3 m downstream of the inlet box (Fig. 1). The UVP was positioned 0.11 m above the bed, angled 60° relative to the local bed slope (Fig. 4a). UVP data acquisition settings are provided in supplementary material Tab. S1. The UVP measures velocities of the suspended particles along the beam-axis, and converted into a bed-parallel component with the assumption that the bed-normal component is ~0 m/s (Fig. 4a), which is suitable for bypass conditions (Sequeiros et al., 2018).

A time-averaged velocity profile was calculated from the body of the current, which is associated with steady-flow conditions. The start of this averaging window was set to ~10 s after the current entered the flume tank after the current-head passed through. The duration of the time averaging was ~80 s (i.e. ~10 s before the end of the experiment). Figure 4b illustrates

the parameterization of the time-averaged velocity profile, where z is the coordinate is positive away from (and normal to) the bed, u is the bed-parallel velocity component, and U_{max} the velocity maximum of the flow. The flow thickness h was defined as the height at which the velocity u is half the velocity maximum U_{max} (Launder and Rodi, 1983).

Samples were collected with siphoning 2.5 m downstream of the inlet box (i.e. 0.2 m downstream of the UVP), at four different elevations above the flume-tank floor (1 cm, 2 cm, 4 cm, and 8 cm) (Fig. 1). The siphon-tube diameter was 7 mm and the average flow velocity in the tube was set to approximately 1 m/s, similar to the velocity scale of the turbidity current. Siphoning commenced ~10 s after the turbidity current entered the flume tank, after the current-head passed through, and was continued until $2*10^{-3}$ m³ of mixture was sampled. The volume and weight of each siphon-tube sample were measured, and sediment concentration was calculated from the bulk density of the sample and the specific densities of the water and sediment. A concentration profile was calculated from the best fit of a three-parameter exponential function through the four concentration measurement points, which is defined as:

$$c(z) = \mathrm{e}^{\frac{(z-l_1)}{-l_2}} - l_3 \,, \tag{6}$$

where the sediment concentration at height z is represented by $c(z)$; l_1, l_2, and l_3 are parameters for the curve fitting.

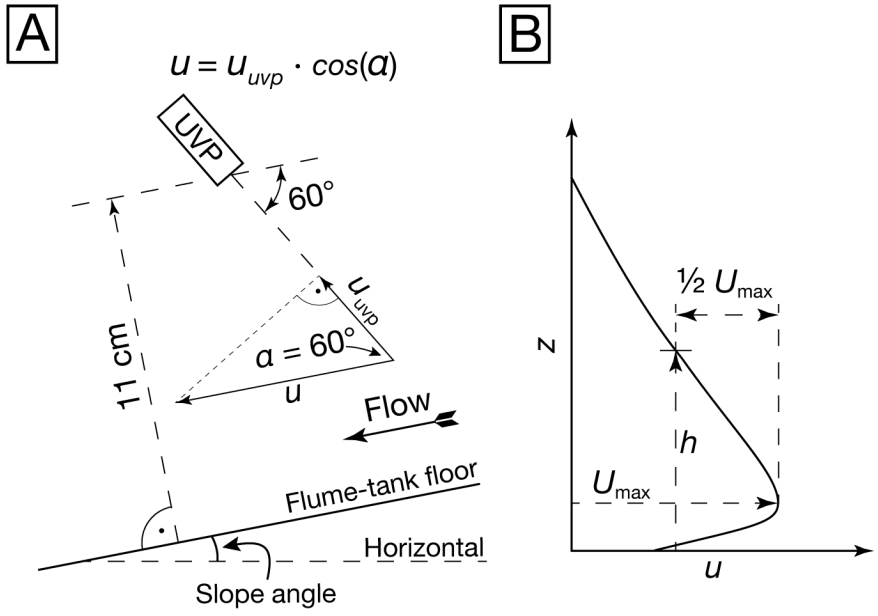

Fig. 4. (a) The orientation of the UVP and the trigonometric calculation to calculate bed-parallel velocities u. The velocity component directed toward the UVP is u_{uvp}. Not to scale. (b) Sketch of a time-averaged velocity profile illustrating the parameterization of the velocity structure. Redrawn and modified from Launder and Rodi (1983).

3. Results

3.1. Depositional patterns

Variation in the steepness of the upper and lower slope resulted in a variety of different depositional behaviors, ranging from high rates of deposition through to bypassing. If deposition occurred, the deposits increased in thickness in downstream direction, away from the location of the UDPO.

3.1.1. Location of the up-dip pinch-out (UDPO)

The location of the UDPO was controlled by the steepness of the upper slope. Steepening of the upper slope resulted in the UDPO position moving further downdip (Figs. 5a and c). Analysis of all of the depositional experiments revealed that with a dipping angle of the upper slope of 5° or less, the UDPO migrated updip of the slope break, If, however, the steepness of the upper slope was 6° or higher, the UDPO was located on the lower slope, and deposits were detached from the upper slope. A variation in steepness of the lower slope caused no shift of the location of the UDPO (Figs. 5b and d).

3.1.2. Deposit-Thickness-Increase (DTI)

A variation in the steepness of the upper slope resulted in a minor signal in the DTI (Figs. 6a and c). In contrast, a variation in the steepness of the lower slope had a signifficant effect on the DTI, where steepening of the lower slope generally resulted in a decreased DTI (Figs. 6b and d).

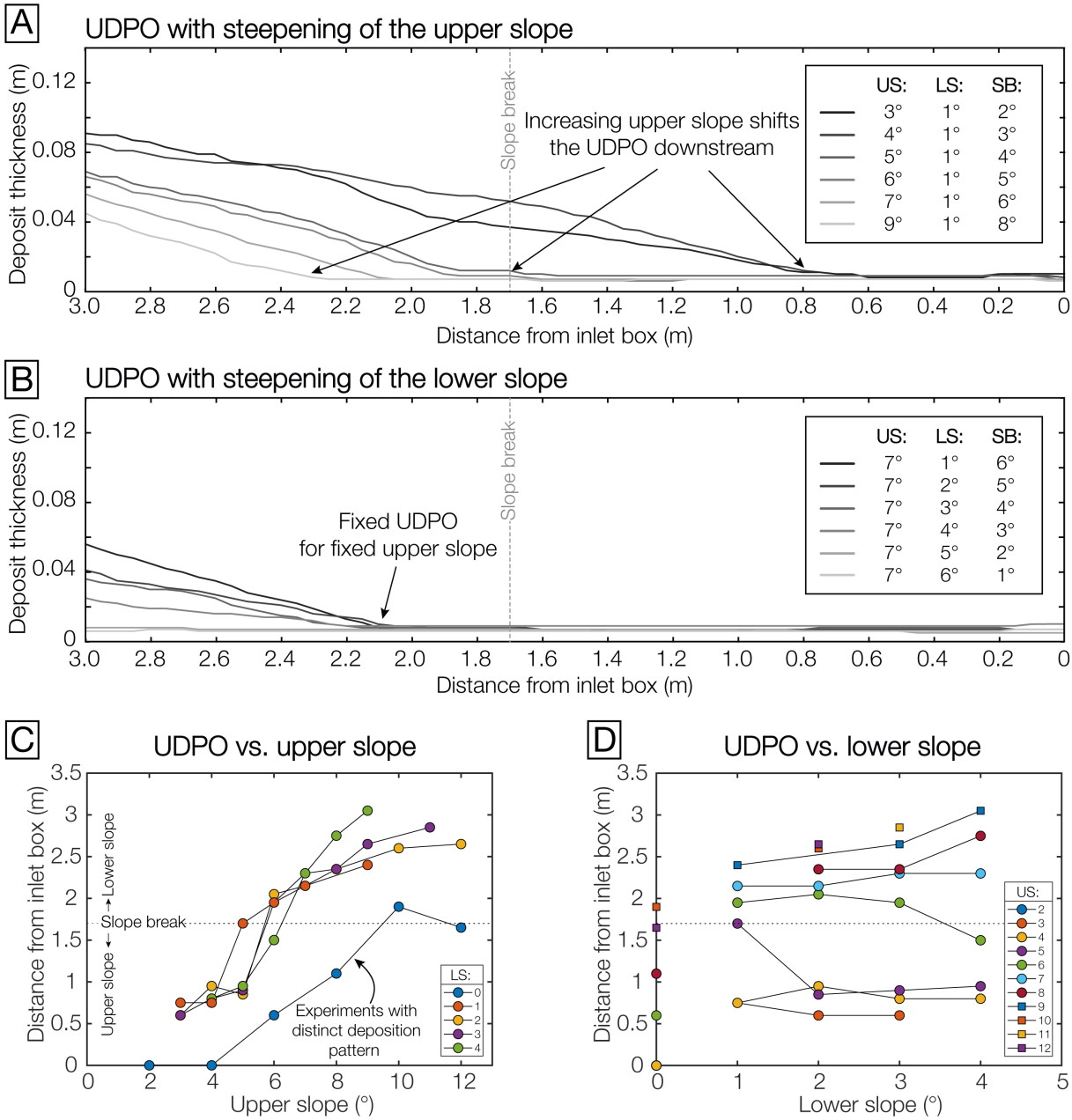

Fig. 5. (a) Depositional profiles of representative experiments, where only the upper slope was varied, and (b), where only the lower slope was varied (cf. Fig. 2). The dipping angles of the upper and lower slopes are restored to horizontal. The profiles were measured along the length of the flume tank and flow direction was from right to left. The slope break was located 1.7 m downstream from the inlet box. (c) The location of the UDPO of all depositional experiments against the steepness of the upper slope, and (d) against the steepness of the lower slope. US: Upper slope, LS: Lower slope, SB: Slope break. Depositional profiles of all of the experiments are shown in the supplementary material Fig. S2.

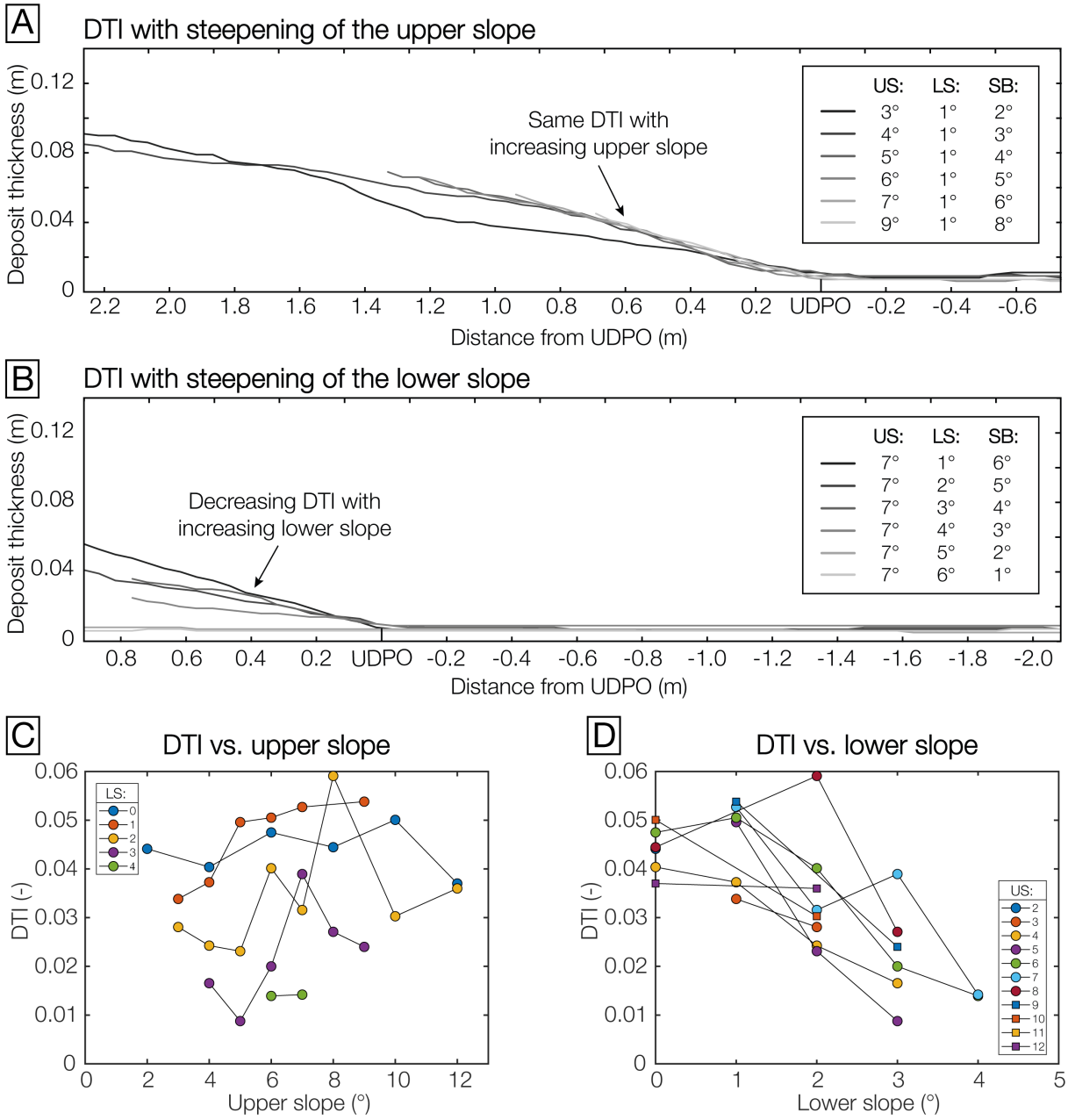

Fig. 6. (a) Depositional profiles of representative experiments, where only the upper slope was varied, and (b), where only the lower slope was varied (cf. Fig. 2). The dipping angles of the upper and lower slopes are restored to horizontal. The deposit profiles were aligned with respect to the location of the UDPO, which was done by a shift of individual profiles along the horizontal axis. (c) The DTI of all depositional experiments against the steepness of the upper slope, and (d) against the steepness of the lower slope. US: Upper slope, LS: Lower slope, SB: Slope break. Depositional profiles of all of the experiments are shown in the supplementary material Fig. S2.

3.1.3. Experiments with a horizontal lower slope

Six experiments were conducted on a horizontal lower slope, where rapid accretion of sediment formed an adverse topographic gradient for the current, resulting in a significant deceleration of the flow. In four of those experiments with an upper slope between 2 to 8°, videos revealed the formation of a roller structure during the last ~10 to 20 s of the experiments (Fig. 7a and supplementary material Video S1). The roller structure was generated at the thickest point of the accreted sediment, 3.1 m downstream of the inlet box, and propagated in an upstream direction. The roller structure was marked by in normally-oriented velocities and deposition rates downstream of the roller structure increased significantly, which resulted in a distinct depositional pattern for these experiments (Fig. 5c and supplementary material Fig. S2). In the other two experiments involving a horizontal lower slope but with steeper upper slopes (i.e. 10 and 12°) no roller structure emerged. Yet towards the end of the experiments, when the flow waned, some of the deposited sediment mobilized on the upstream-dipping slope and moved in a direction opposed to the original flow direction, and thus, overprinted the original depositional pattern (Fig. 5c and supplementary material Fig. S2). In other experiments, on steeper lower slopes and with less depositional flows, no roller structure or sediment mobilization occurred (Fig. 7b and supplementary material Video S2).

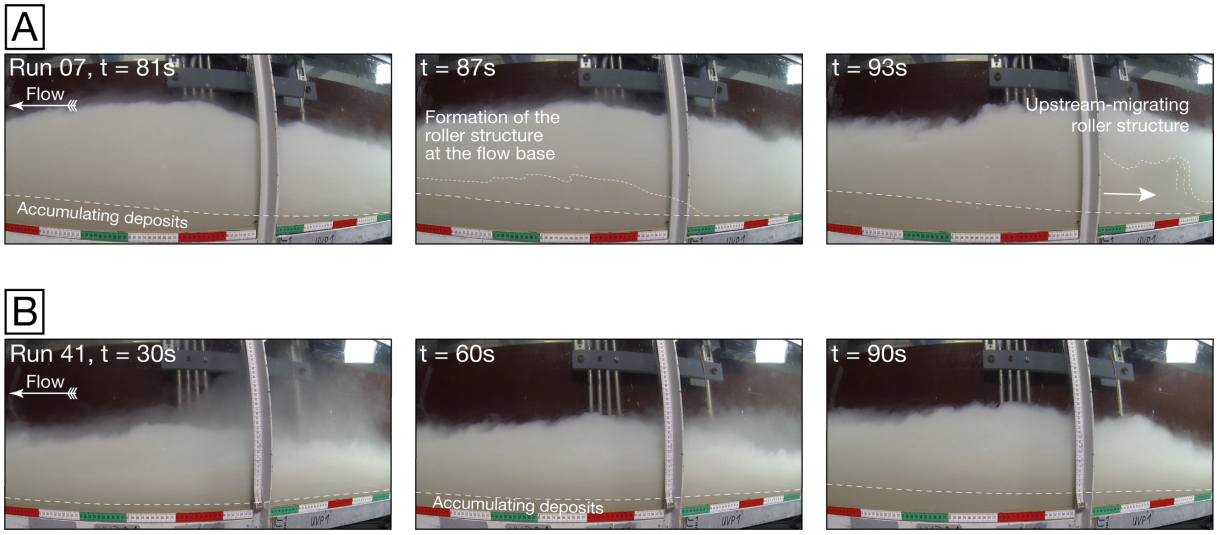

Fig. 7. Snapshots of videos from the flow through the glass side-wall of the flume tank; see Figure 1 for field of view. (a) An experiment in which a roller structure emerged on the deposits and migrated upstream. In the experiment, the upper slope was 8° and the lower slope was horizontal. (YouTube: https://youtu.be/Ny-TN7HMYs0) (b) A typical experiment in which sediment was deposited, but no roller structure emerged. In this experiment, the upper slope was 6° and the lower slope was 1°. The green, red, and white scale bars are each 0.1 m long. (YouTube: https://youtu.be/PMCtaZyj0Ts).

3.2. Flow dynamics in the bypass-slope experiment

The flow in the bypass-slope experiment accelerated as it flowed through the flume tank. The depth-averaged velocity of ~0.81 m/s at the inlet box was increased to 0.93 m/s at the UVP (i.e. 2.3 m further downstream). The time-averaged velocity profile of the turbidity current obtained by the UVP is shown in Figure 8a. The velocity maximum (U_{max}) was 1.15 m/s, at a height that was elevated 1.6 cm above the bed. Flow thickness (h) was 5.4 cm.

The vertical sediment concentration profile showed a stratification with decreasing concentration towards the top of the flow (Fig 8b). The sediment concentration of the initial mixture of 17 %vol was decreased to a depth-averaged sediment concentration (C) 13.7 %vol at the siphon tubes (i.e. 2.5 m further downstream).

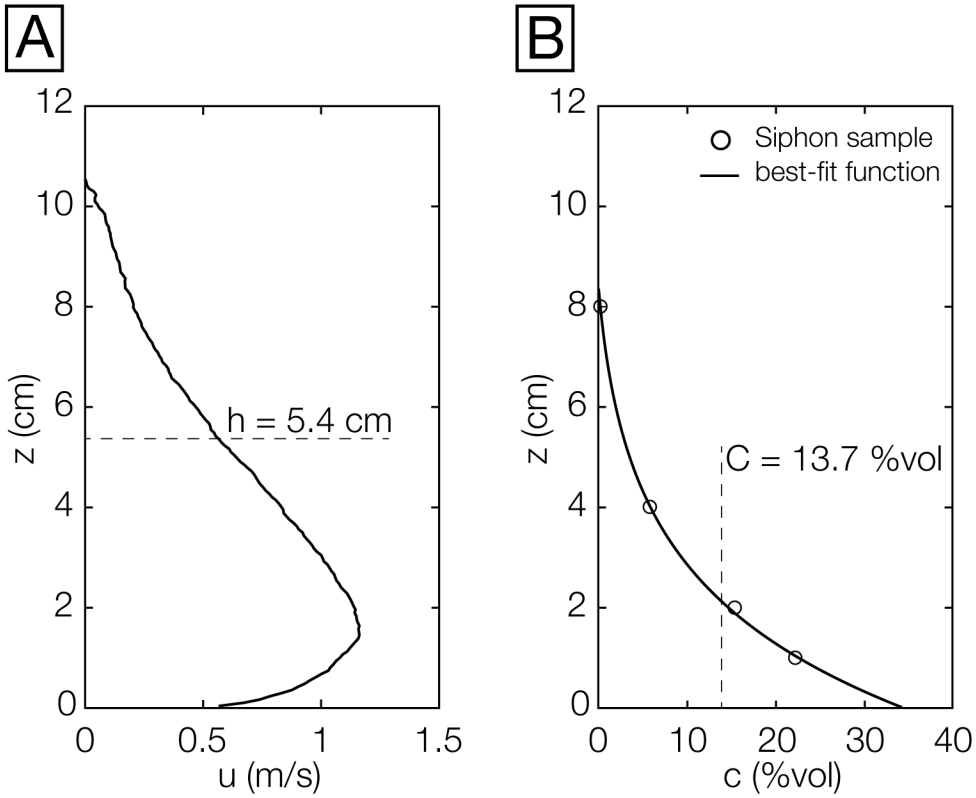

Fig. 8. (a) Time-averaged velocity profile and, (b) sediment concentration profile of the turbidity current in the bypass-slope experiment.

4. Discussion

4.1. Control mechanisms on the UDPO and the DTI

The main research objective of this study is to examine how the location of the UDPO and the DTI in a slope-break system are controlled by the system's geometry. Geometric parameters in a slope-break system are the steepness of the upper and the lower slopes, and how these two free variables interact to determine the severity of the slope break.

The steepness of the upper slope is the primary control on the location of the UDPO; steeper upper slopes force the location of the UDPO farther downdip (Figs. 5c and 9a). This suggests that the bypass-slope criterion (i.e. the most gently-dipping slope angle at which a given turbidity current is still bypassing its sediment load) can be used as a predictor of slope-detached sedimentation patterns. In slope-break systems with an upper slope that is gentler dipping than the bypass-slope criterion, the deposits may onlap onto the upper slope due to the reduction in the turbidity current's transport potential. For slope-break systems with upper slopes greater or equal to the bypass-slope criterion, the UDPO will be located downdip of the slope break, on the lower slope.

The location of the UDPO is also controlled by the efficiency of the flow in its sediment transportation capability (Mutti, 1992). The flow efficiency is controlled by the grain-size distribution of the suspended sediment, the flow volume, and the flow density (Al Ja'Aidi et al., 2004; Mutti, 1992). Large, finer grained flows with a high density are more efficient than smaller, coarser grained flows with a low density (Al Ja'Aidi et al., 2004; Mutti, 1992). High-efficient flows transport their sediment load further into the basin before deposition commences, and hence, the UDPO is located further downstream. Conversely, the position of the UDPO deposited by a low-efficient flow will be located further upstream.

In contrast to the position of the UDPO, which is governed by the upper slope and therefore results from upstream controls, the DTI is dictated by the lower slope, and therefore results from downstream controls in a slope-break system. A steeper dipping lower slope resulted in a lower DTI and, consequently, thinner deposits on the lower slope (Figs. 6d and 9b). On a gentler dipping lower slope, the flow has less sediment transport capability resulting in thicker deposits.

In our experiments, slope-break settings with a horizontal lower slope represent a geometrical arrangement, which results in a distinct depositional pattern (cf. Fig. 5c) related to high sedimentation rates on the horizontal lower slope. A horizontal lower slope was also used in all previous experimental studies involving a slope break (Garcia and Parker, 1989; Garcia, 1994; Gray et al., 2005; Islam and Imran, 2010; Mulder and Alexander, 2001). Our results suggest that slope-break systems with a horizontal lower slope represent an exceptional condition since it's the only geometrical arrangement where gravitational forces lack a downflow component, and that these systems need to be assessed separately.

The severity of the slope break is an inadequate parameter to describe the system's geometry since it can represent a variety of different upper and lower slope combinations (cf. Fig.2). Our results indicate that the severity of the slope break, as a parameter, has no discernable impact

on the depositional pattern. These findings may challenge the interpretations of previous studies, where variations in flow dynamics or depositional patterns are associated with the severity of the slope break (Gray et al., 2005; Mulder and Alexander, 2001). In these studies, the increase in severity of the slope break was achieved by steepening of the upper slope, while the lower slope was kept horizontal. Hence, variations in flow dynamics or depositional patterns are likely to be caused by the steepening of the upper slope, rather than the increasing severity of the slope break.

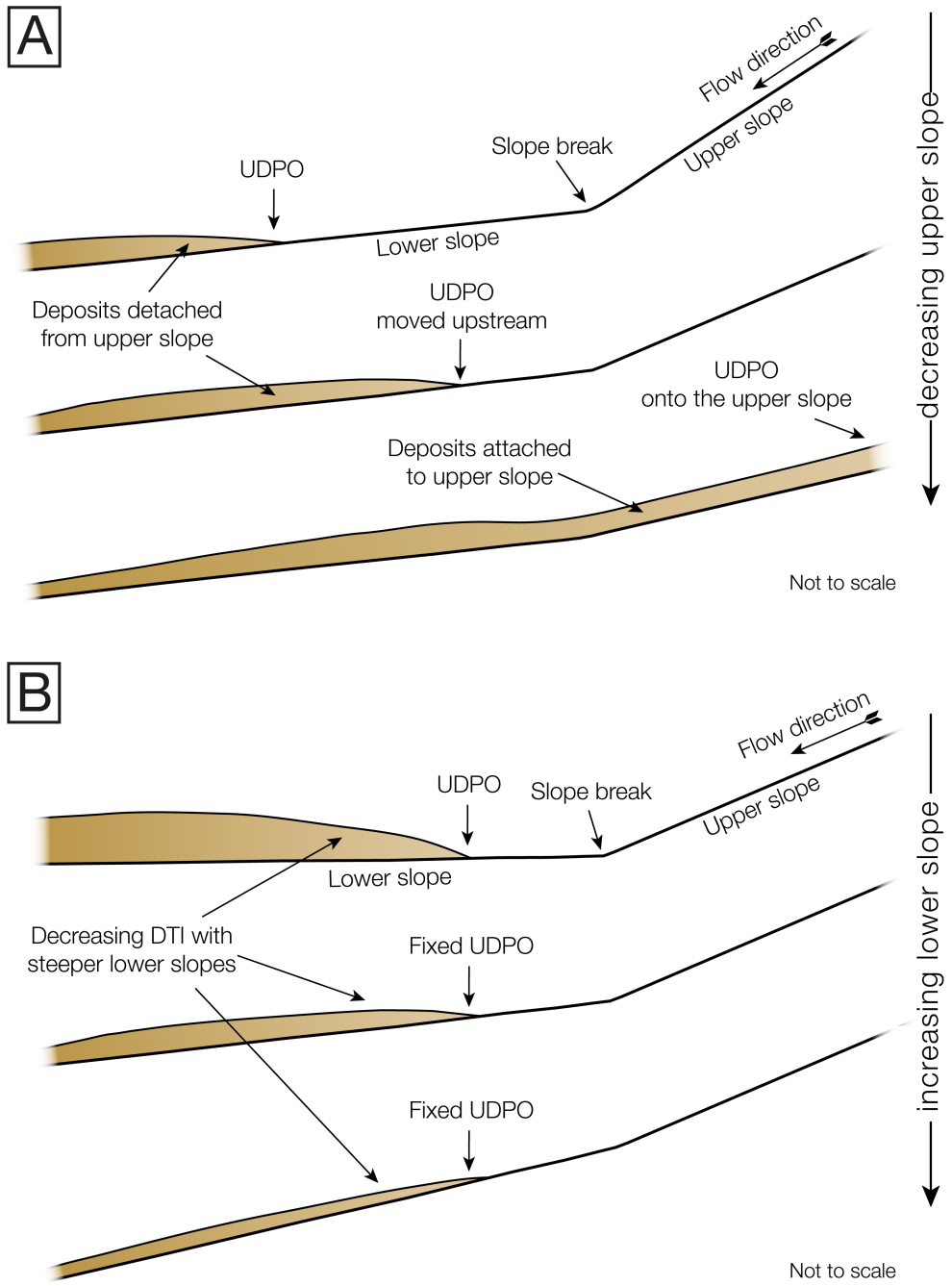

Fig. 9. Sketch illustrating the impact of the upper and lower slopes on the depositional pattern in a slope-break system. (a) Upstream shift of the UDPO position due to the decrease of the upper slope. (b) Decrease of the DTI due to the increase of the lower slope.

The present study has considered the effects of a slope break on the depositional signal of turbidity currents. It is important to note that a slope break can be accompanied by a loss in lateral confinement in natural systems (Wynn et al., 2002), which would create an overprint on the depositional pattern reported herein (Alexander et al., 2008; Stacey et al., 2018). Future studies are required to assess the relative contribution of these two factors in the depositional record.

4.2. Scaling to natural flows and systems

Experimental turbidity currents are, by definition, much smaller than natural turbidity currents. For example, measurements of natural flows reveal flow thicknesses of ~20 – 150 m, which are orders of magnitude larger than the modeled turbidity currents created in this study (Azpiroz-Zabala et al., 2017; Khripounoff et al., 2003, 2012, Xu et al., 2004, 2010, 2014). In contrast to that, the depth-averaged sediment concentration of natural flows can be ~500 times lower than the concentration of the modeled flows (Azpiroz-Zabala et al., 2017; Xu et al., 2014). In this section we scale the bypass-slope criterion of the modeled turbidity currents to natural values and test, whether the modeled flow resemble the depositional behavior of monitored natural turbidity currents.

The fundamental scaling parameter for the Shield scaling is the Shields parameter, which is kept close to natural values:

$$\theta_{Nat} = \theta_{Exp} \quad . \tag{7}$$

The subscript *Nat* represents the values of a natural turbidity current and *Exp* the values of the experimental current presented herein. By substituting Equation 5 into Equation 7 gives:

$$\frac{C_{Nat} h_{Nat} S_{Nat}}{d_{t\,Nat}} = \frac{C_{Exp} h_{Exp} S_{Exp}}{d_{t\,Exp}} \quad . \tag{8}$$

Equation 8 allows scaling of the experimental conditions to natural values, to see which natural settings can be expected to obey the observed depositional patterns.

We scale the bypass-slope conditions of the experiments to natural values by using the flow thickness (h_{Nat}), the grain size of the suspended sediment (d_{tNat}), and the sediment concentration (C_{Nat}) of monitored natural turbidity currents on the ocean floor. Although there is a rising number of measurements on natural turbidity currents (Hughes Clarke, 2016; Khripounoff et al., 2012, 2003; Liu et al., 2012; Paull et al., 2018; Xu et al., 2010, 2004; Zhang et al., 2018), so far only two studies provide a full range of measurements, including the thickness (h) and the sediment concentration (C) of the flow (Azpiroz-Zabala et al., 2017; Xu et al., 2014). In these studies, flows in the Congo Canyon (Azpiroz-Zabala et al., 2017) and the Monterey Canyon (Xu et al., 2014) were monitored, which will be herein used for scaling (Tab. 1).

	Event	Measured slope	Sediment concentration	Flow height	Median grain size	Bypass-slope (Scaled)	Predicted flow behaviour
	–	(°)	(%vol)	(m)	(µm)	(°)	–
Flume experiment	Bypass-slope experiment	6	13.7	0.054	133	6	–
Congo Canyon (Azpiroz-Zabala et al., 2017)	1	0.14 – 0.29	0.018	53	100	3.5	Depositional
	2	0.14 – 0.29	0.02	57	100	2.9	Depositional
	3	0.14 – 0.29	0.02	48	100	3.5	Depositional
	4	0.14 – 0.29	0.023	69	100	2.1	Depositional
	5	0.14 – 0.29	0.02	77	100	2.2	Depositional
	6	0.14 – 0.29	0.017	68	100	2.9	Depositional
	Average	0.14 – 0.29	0.02	62	100	2.7	Depositional
Monterey Canyon (Xu et al., 2014)	TC 1; R2	1.7	0.02	52.5	100	3.2	Depositional
	TC 1; R3	2.9	0.04	57.1	100	1.5	Bypassing
	TC 2; R1	1.7	1.36	23.9	100	0.1	Bypassing
	TC 2; R2	1.7	0.11	38.2	100	0.8	Bypassing
	TC 3; R3	2.9	0.16	31.1	100	0.7	Bypassing
California Margin (Assumtions based on Lee et al., 2002)	–	~20	0.02	25	100	6.7	Bypassing
Numerical simulations, Niger Delta slope, Channel X (Abd El-Gawad et al., 2012)	1	0.57	1.25	35	30	0.02	Bypassing
	2	0.57	1.25	35	64	0.05	Bypassing
	3	0.57	1.25	35	125	0.1	Bypassing
	4	0.57	1.25	35	250	0.19	Bypassing
	5	0.57	1.25	55	30	0.01	Bypassing
	6	0.57	1.25	55	64	0.03	Bypassing
	7	0.57	1.25	55	125	0.06	Bypassing
	8	0.57	1.25	55	250	0.12	Bypassing

Tab. 1. Flow parameters used for the scaling of the bypass-slope criterion of the flow in the bypass-slope experiment to natural turbidite systems.

The scaled bypass-slopes condition in Table 1 describe the minimum slope on which natural flows with the given conditions would bypass. Hence, the monitored turbidity currents in the Congo Canyon are likely to deposit, since the scaled bypass-slope condition is steeper than the actual slope of the canyon (Tab. 1). The turbidity currents monitored in the Congo Canyon are presumed to be depositional, which would conform with our predicted behavior (Azpiroz-Zabala et al., 2017). In the Monterey Canyon, the scaled bypass-slope condition, of the majority of the flows, is less than the actual slope of the canyon floor, suggesting bypass at this location. For some of the flows the scaled bypass-slope criterion is significantly steeper than the actual slope of the canyon floor, suggesting vigorous bypass and erosion. This predicted flow behavior corresponds to the predominantly erosional geomorphic evolution of the Monterey Canyon, as revealed by a series of bathymetry surveys (Smith et al., 2007). In addition, observations by remotely operated vehicles in the Monterey Canyon, revealed a scoured canyon thalweg and a lack of colonization by encrusting organisms, indicating recent abrasion and sediment bypass (Paull et al., 2011). Entrainment of sediment due to erosion would result in changes of the flow parameters and, therefore, the bypass-slope criterion of that flow. However, we did not test the effect of erosion in our experiments, since they were conducted with a non-erodable flume tank floor.

4.3. Application to natural slope-break systems

4.3.1. Stratigraphic development of slope-break systems

Above-grade slope systems (*sensu* Prather, 2000) may have longitudinal profiles involving multiple slope breaks. There are two types of above-grade slope systems: stepped slopes, characterized by a low relief or terraced topography, and ponded slopes, characterized by the presence of enclosed intra-slope basins (Prather et al., 2017). Here we demonstrate how Shields scaling can be applied to the stratigraphic record to explain the system's morphologic evolution. For this we use as an example for a system with a slope-detached sedimentation pattern the Niger Delta slope, and for a slope-attached sedimentation pattern the Brazos-Trinity Turbidite System in the Gulf of Mexico.

The Niger Delta slope is an above-grade slope system with a stepped slope topography (Adeogba et al., 2005; Beaubouef and Friedmann, 2000; Jobe et al., 2017; Prather et al., 2012a). Each step represents a slope break and forms a small catchment area for sediment. These catchment areas are is infilled with perched submarine aprons, resulting in a healed-slope profile and disappearance of the step over time. The perched submarine apron (OML 134) is subdivided into a lower apron and an overlying upper apron (Prather et al., 2012a) (Fig 10a). At the basin entry point, which corresponds to the slope break, the lower apron is characterized by multiple erosional features. These erosional features suggest a slope-detached depositional style for the lower apron. Based on numerical modeling of the potential flows in the feeder channel of the apron OML 134 (Abd El-Gawad et al., 2012), we calculated a bypass-slope criterion of 0.01 to 0.19° (Tab. 1). The range for the possible bypass-slope criterion is, indeed, below the actual slope of 0.57° in the channel thalweg (Abd El-Gawad et al., 2012), corroborating the suggested slope-detached sedimentation. In contrast to the erosional features

observed in the lower apron, the upper apron is perched over the sediments of the lower apron (Prather et al., 2012a). Hence there was a switch in terms of flow behavior from an erosive to a depositional pattern. The reason for this change may have been due to changes in the geometry of the slope-break system as the basin was infilled with sediment. However, according to our model, in such a case the sedimentation style of the upper apron should still be dominated by erosion and bypass, since the steepness of the slope of the incoming channel was kept constant as the basin was infilled. Nonetheless, variations in flow properties, like flow thickness and grain size, affect the value of the bypass-slope criterion and will contribute to the stratigraphic evolution of the system, as for example described for the evolution of channel systems (Jobe et al., 2015).

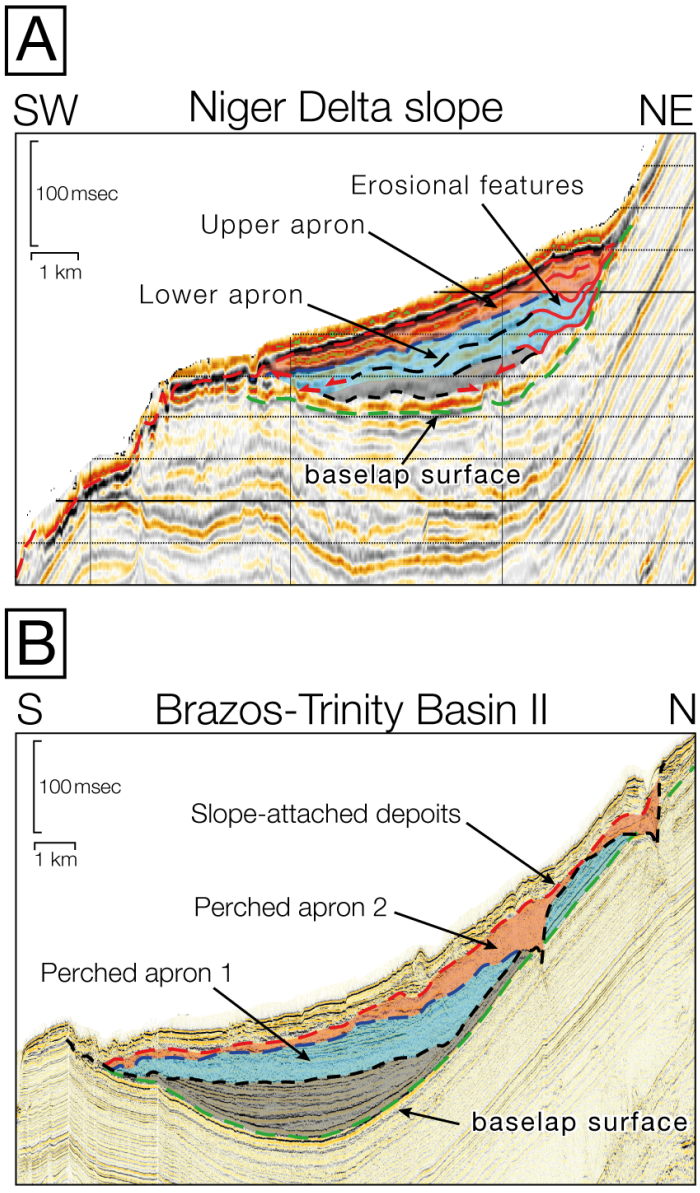

Fig. 10. (a) Seismic cross-section of the Niger Delta slope as example for a slope-detached sedimentation pattern. The red lines indicate erosive contacts at the slope break (i.e. the basin entry point). Modified after: Prather et al. (2012a). (b). Seismic cross-section of the Brazos-Trinity Basin II as example for slope-attached sedimentation with less scour development and an onlapping sedimentation pattern. Modified after: Prather et al. (2012b).

The Brazos-Trinity Turbidite System, offshore Gulf of Mexico, is an above-grade ponded-slope system (Badalini et al., 2000; Prather et al., 1998, 2017, 2012b; Winker, 1996). The Brazos-Trinity Turbidite System consists of four intra-slope basins, which are connected by a channel system (Prather et al., 2012b). The proximal region of each ponded basin is characterized by a slope break, affecting the basin's sedimentation style. A seismic section through the Brazos-Trinity Basin II reveals a succession of perched aprons onlapping onto the upstream slope (Fig. 10b). This infilling pattern differs from that of the Niger Delta slope, in that it shows no erosion at the basin entry point (Prather et al., 2012a). Hence, the slope of the incoming channel of the Brazos-Trinity Basin II should be gentler than the bypass slope of the typical flows in that system. We were, however, not able to estimate reasonable values for the bypass-slope criterion due to the lack of precise geometric information. Nonetheless, the slope of the Brazos-Trinity Turbidite System appears to be gentler than that of the Niger Delta slope (Prather et al., 2017). It might, therefore, be plausible that the channel slope is gentler than the bypass-slope criterion, resulting in the onlapping pattern of the perched aprons in the Brazos-Trinity Basin II.

Shield scaling provides an additional tool for the risk estimation of hydrocarbon reservoirs in slope-break systems. If sandy deposits downstream of a slope break are connected to the up-dip slope sands, potential hydrocarbons leak through those connections. In contrast, a system with slope-detached sand sedimentation may result in the formation of sealed reservoirs (Doré and Robbins, 2005; Ray et al., 2010). The estimation of the bypass-slope criterion and the comparison with the actual upper slope in a slope-break system provides a rough assessment of the likelihood of whether or not deposits drape the upper slope. If the upper slope adjacent to the slope break is steeper than the bypass-slope criterion, deposits are likely to be detached from the upper slope. Conversely, upper slopes that are less steep than the bypass-slope criterion are more likely to form attached deposits, and therefore poorly sealed reservoirs.

4.3.2. Plunge pools

Plunge pools represent an end member slope-break system and usually form in geometric arrangements with a steep upper slope and a severe slope break (Bourget et al., 2011; Lee et al., 2002). The continental slope of the California Margin, for example, is ~20° steep and characterized by a series of gullies that terminate in plunge pools (Lee et al., 2002); similar slope angles have been reported along the Makran system (Bourget et al., 2011). In principle, plunge pools are examples for slope-detached sedimentation pattern. As stated above, the bypass-slope criterion can be used as a predictor of slope-detached sedimentation in a slope-break system. Hence, the upper slope in plunge-pool systems should be steeper than the bypass-slope criterion for the typical turbidity currents in these systems.

Taking the California Margin as an example, we apply the Shields scaling to evaluate the bypass-slope criterion for this plunge-pool system. Unfortunately, flows in the gullies on the California Margin have, to date, not been monitored. Therefore, we assume a similar grain size and sediment concentrations as monitored in the Monterey Canyon, which is located farther south on the California Margin. For the flow thickness, however, we used the depth of the gullies on the California Margin (i.e. 25 m; Lee et al., 2002). The steepest possible scaled

bypass-slope criterion, calculated with the lowest sediment concentration of 0.02 %vol, would be 6.7° (Tab. 1). Since the actual slope on the California Margin is much steeper (~20°) than the estimated bypass-slope criterion, these flows would bypass on the slope and deposit sediment relatively far downstream of the slope break, resulting in the development of a slope-detached sedimentation pattern.

Lee et al. (2002) suggested an abrupt slope break of > 4°as the minimum criterion for the formation of a plunge pool, although observations suggest that plunge pools are well developed at slope breaks of > 15° (Lee et al., 2002). Importantly, the slope break values reported in the literature are based entirely on empirical observations. In contrast, Shields scaling provides an analytical framework for developing a criterion for the development of plunge pools based on the flow properties of turbidity currents and the calculation of bypass-slope criterion. Based on our experimental work, it appears that slope-break severity alone cannot explain plunge pool formation. Instead, we suggest that the criterion for the formation of a plunge pool would be an upper slope angle that is steeper than the bypass-slope criterion and a gently dipping or horizontal lower slope, resulting in a severe slope break.

5. Conclusions

The Shields-scaled experiments of the present study are the first experiments which have mimicked the transition from a bypassing to a depositional turbidity current in a slope-break system. Furthermore, we presented the first experiments involving a dipping, non-horizontal lower slope, downstream of the slope break, as well as testing a variety of 45 different combinations of the upper and lower slopes.

1) The geometric control parameters in a slope-break system are the steepness of the upper and lower slope. Our results show that the severity of the resulting slope break, as a parameter, shows no clearly discernible impact on the depositional pattern, since it represents a variety of different upper and lower slope combinations. Therefore, we suggest that in a slope-break system, it is not the severity of the slope break which should be considered as the main parameter or driving factor in this system, but rather the combination of the incoming, upper and outgoing lower slopes.

2) In our experiments slope-break systems with a horizontal lower slope resulted in high sedimentation rates on the horizontal lower slope and the formation of a roller structure, producing a distinctly different depositional pattern. Furthermore, are gravitational forces lacking a downflow component on a horizontal lower slope. Hence, slope-break systems with a horizontal lower slope are likely to represent an exceptional condition and should, therefore, be considered separately form slope-break systems with dipping lower slopes.

3) In a slope-break system the location of the UDPO is controlled by the upper slope, whereas the value of the DTI is controlled by the lower slope. An increase in the angle of the upper slope shifts the UDPO basinwards making the connection between

basin floor sediments and slope sediments less likely. Increasing the angle of the lower slope results in thinner deposits, but has no impact on the location of the UDPO.

4) Shields scaling can be used to scale the bypass-slope criterion of the modeled turbidity currents to that of natural turbiditic systems. For this, the flow thickness, sediment concentration, and grain size of a natural system need to be known or assumed. The herein presented scaling approach provides a tool to predict whether or not the steepness of a slope is sufficient to cause sediment bypass conditions for a certain flow. This may be useful for the risk estimation of potential hydrocarbon reservoirs in slope-break systems.

Nomenclature

C	Depth-averaged sediment concentration (%vol)
c	Sediment concentration (%vol)
d_b	Grain size of the sediment bed (m)
d_t	Grain size of the suspended sediment (m)
g	Acceleration by gravity (9.81 m/s²)
h	Flow thickness (m)
$l_{1,2,3}$	Curve fitting parameters (-)
ρ_t	Density of the turbidity current (kg/m³)
ρ_s	Density of sediment (2650 kg/m³)
ρ_w	Density of water (1000 kg/m³)
θ	Shields parameter (-)
Re_p	Reynolds particle number (-)
S	Tangent of the slope (-)
u	Velocity (m/s)
U_{max}	Velocity maximum (m/s)
u_{uvp}	Velocity directed toward the UVP (m/s)
u_*	Shear velocity (m/s)
ν	Kinematic viscosity ($1*10^{-6}$ m²/s)
z	Coordinate directed upward normal to the bed (m)

References

Abd El-Gawad, S., Cantelli, A., Pirmez, C., Minisini, D., Sylvester, Z., Imran, J., 2012. Three-dimensional numerical simulation of turbidity currents in a submarine channel on the seafloor of the Niger Delta slope. J. Geophys. Res. Ocean. 117, 1–16. https://doi.org/10.1029/2011JC007538

Adeogba, A.A., McHargue, T.R., Graham, S.A., 2005. Transient fan architecture and depositional controls from near-surface 3-D seismic data, Niger Delta continental slope. Am. Assoc. Pet. Geol. Bull. 89, 627–643. https://doi.org/10.1306/11200404025

Al Ja'Aidi, O.S., McCaffrey, W.D., Kneller, B.C., 2004. Factors influencing the deposit geometry of experimental turbidity currents: implications for sand-body architecture in confined basins. Geol. Soc. London, Spec. Publ. 222, 45–58. https://doi.org/10.1144/GSL.SP.2004.222.01.04

Alexander, J., McLelland, S.J., Gray, T.E., Vincent, C.E., Leeder, M.R., Ellett, S., 2008. Laboratory sustained turbidity currents form elongate ridges at channel mouths. Sedimentology 55, 845–868. https://doi.org/10.1111/j.1365-3091.2007.00923.x

Amy, L., Kneller, B., McCaffrey, W., 2000. Evaluating the Links Between Turbidite Characteristics and Gross System Architecture: Upscaling Insights from the Turbidite Sheet-System of Peïra Cava, SE France. Deep. Reserv. World 20th Annu. 1–15. https://doi.org/10.5724/gcs.00.15.0001

Azpiroz-Zabala, M., Cartigny, M.J.B., Talling, P.J., Parsons, D.R., Sumner, E.J., Clare, M.A., Simmons, S.M., Cooper, C., Pope, E.L., 2017. Newly recognized turbidity current structure can explain prolonged flushing of submarine canyons. Sci. Adv. 3, 1–12. https://doi.org/10.1126/sciadv.1700200

Badalini, G., Kneller, B., Winker, C.D., 2000. Architecture and process in the Late Pleistocene Trinity–Brazos turbidite system, Gulf of Mexico, in: Weimer, P., Slatt, R.M., Coleman, J., Rosen, N.C., Nelson, H., Bouma, A.H., Styzen, M.J., Lawrence, D.T. (Eds.), Deep-Water Reservoirs of the World: Gulf Coast Section. SEPM Foundation, 20th Annual Bob F. Perkins Research Conference, pp. 16–34.

Beaubouef, R.T., Friedmann, S.J., 2000. High Resolution Seismic/Sequence Stratigraphic Framework for the Evolution of Pleistocene Intra Slope Basins, Western Gulf of Mexico: Depositional Models and Reservoir Analogs. Deep. Reserv. World 20th Annu. 40–60. https://doi.org/10.5724/gcs.00.15.0040

Bourget, J., Zaragosi, S., Ellouz-Zimmermann, N., Mouchot, N., Garlan, T., Schneider, J.L., Lanfumey, V., Lallemant, S., 2011. Turbidite system architecture and sedimentary processes along topographically complex slopes: The Makran convergent margin. Sedimentology 58, 376–406. https://doi.org/10.1111/j.1365-3091.2010.01168.x

Brooks, H.L., Hodgson, D., Brunt, R.L., Peakall, J., Hofstra, M., Flint, S., 2018. Deepwater channel-lobe transition zone dynamics — processes and depositional architecture, an example from the Karoo Basin, South Africa. Geol. Soc. Am. Bull. https://doi.org/10.1130/B31714.1

Cartigny, M.J.B., Eggenhuisen, J.T., Hansen, E.W.M., Postma, G., 2014. Concentration-Dependent Flow Stratification In Experimental High-Density Turbidity Currents and Their Relevance To Turbidite Facies Models. J. Sediment. Res. 83, 1046–1064. https://doi.org/10.2110/jsr.2013.71

Carvajal, C.R., Steel, R.J., 2006. Thick turbidite successions from supply-dominated shelves during sea-level highstand. Geology 34, 665–668. https://doi.org/10.1130/G22505.1

Daly, R.A., 1936. Origin of Submarine "Canyons." Am. J. Sci. 31, 401–420. https://doi.org/10.2475/ajs.s5-31.186.401

de Leeuw, J., Eggenhuisen, J.T., Cartigny, M.J.B., 2018a. Linking submarine channel–levee facies and architecture

to flow structure of turbidity currents: insights from flume tank experiments. Sedimentology 65, 931–951. https://doi.org/10.1111/sed.12411

de Leeuw, J., Eggenhuisen, J.T., Cartigny, M.J.B., 2016. Morphodynamics of submarine channel inception revealed by new experimental approach. Nat. Commun. 7, 1–7. https://doi.org/10.1038/ncomms10886

de Leeuw, J., Eggenhuisen, J.T., Spychala, Y.T., Heijnen, M.S., Pohl, F., Cartigny, M.J.B., 2018b. Sediment Volume and Grain-Size Partitioning Between Submarine Channel−Levee Systems and Lobes: An Experimental Study. J. Sediment. Res. 88, 777–794. https://doi.org/10.2110/jsr.2018.46

Doré, G., Robbins, J., 2005. The Buzzard Field, in: Doré, A.G., Vining, B.A. (Eds.), Petroleum Geology: North-West Europe and Global Perspectives – Proceedings of the 6th Petroleum Geology Conference. The Geological Society, London, pp. 241–252.

Garcia, M., 2008. Sedimentation Engineering: Processes, Measurements, Modeling and Practise. Am. Soc. Civ. Eng.

Garcia, M., Parker, G., 1989. Experiments on hydraulic jumps in turbidity currents near a canyon-fan transition. Science (80-.). 245, 393–396. https://doi.org/10.1126/science.245.4916.393

Garcia, M.H., 1994. Depositional Turbidity Currents Laden with Poorly Sorted Sediment. J. Hydraul. Eng. 120, 1240–1263. https://doi.org/10.1061/(ASCE)0733-9429(1994)120:11(1240)

Garcia, M.H., 1993. Hydraulic Jumps in Sediment-Driven Bottom Currents. J. Hydraul. Eng. 119, 1094–1117. https://doi.org/10.1061/(ASCE)0733-9429(1993)119:10(1094)

Gray, T.E., Alexander, J., Leeder, M.R., 2006. Longitudinal flow evolution and turbulence structure of dynamically similar, sustained, saline density and turbidity currents. J. Geophys. Res. Ocean. 111, 1–14. https://doi.org/10.1029/2005JC003089

Gray, T.E., Alexander, J., Leeder, M.R., 2005. Quantifying velocity and turbulence structure in depositing sustained turbidity currents across breaks in slope. Sedimentology 52, 467–488. https://doi.org/10.1111/j.1365-3091.2005.00705.x

Hermidas, N., Eggenhuisen, J.T., Jacinto, R.S., Luthi, S.M., Toth, F., Pohl, F., 2018. A Classification of Clay-Rich Subaqueous Density Flow Structures. J. Geophys. Res. Earth Surf. 123, 945–966. https://doi.org/10.1002/2017JF004386

Hughes Clarke, J.E., 2016. First wide-angle view of channelized turbidity currents links migrating cyclic steps to flow characteristics. Nat. Commun. 7, 1–13. https://doi.org/10.1038/ncomms11896

Islam, M.A., Imran, J., 2010. Vertical structure of continuous release saline and turbidity currents. J. Geophys. Res. Ocean. 115, 1–14. https://doi.org/10.1029/2009JC005365

Jobe, Z.R., Sylvester, Z., Howes, N., Pirmez, C., Parker, A., Cantelli, A., Smith, R., Wolinsky, M.A., O'Byrne, C., Slowey, N., Prather, B., 2017. High-resolution, millennial-scale patterns of bed compensation on a sand-rich intraslope submarine fan, western Niger Delta slope. Bull. Geol. Soc. Am. 129, 23–37. https://doi.org/10.1130/B31440.1

Jobe, Z.R., Sylvester, Z., Parker, A.O., Howes, N., Slowey, N., Pirmez, C., 2015. Rapid Adjustment of Submarine Channel Architecture To Changes In Sediment Supply. J. Sediment. Res. 85, 729–753. https://doi.org/10.2110/jsr.2015.30

Khripounoff, A., Crassous, P., Lo Bue, N., Dennielou, B., Silva Jacinto, R., 2012. Different types of sediment gravity flows detected in the Var submarine canyon (northwestern Mediterranean Sea). Prog. Oceanogr. 106,

138–153. https://doi.org/10.1016/j.pocean.2012.09.001

Khripounoff, A., Vangriesheim, A., Babonneau, N., Crassous, P., Dennielou, B., Savoye, B., 2003. Direct observation of intense turbidity current activity in the Zaire submarine valley at 4000 m water depth. Mar. Geol. 194, 151–158. https://doi.org/10.1016/S0025-3227(02)00677-1

Kneller, B., 2003. The influence of flow parameters on turbidite slope channel architecture. Mar. Pet. Geol. 20, 901–910. https://doi.org/10.1016/j.marpetgeo.2003.03.001

Kneller, B.C., Branney, M.J., 1995. Sustained High-Density Turbidity Currents and the Deposition of Thick Massive Sands. Sedimentology 42, 607–616. https://doi.org/10.1111/j.1365-3091.1995.tb00395.x

Launder, B.E., Rodi, W., 1983. The Turbulent Wall Jet Measurements and Modeling. Annu. Rev. Fluid Mech. 15, 429–459. https://doi.org/10.1146/annurev.fl.15.010183.002241

Lee, S.E., Amy, L.A., Talling, P.J., 2004. The character and origin of thick base-of-slope sandstone units of the Peïra Cava outlier, SE France. Geol. Soc. London, Spec. Publ. 221, 331–347. https://doi.org/10.1144/GSL.SP.2004.221.01.18

Lee, S.E., Tailing, P.J., Ernst, G.G.J., Hogg, A.J., 2002. Occurrence and origin of submarine plunge pools at the base of the US continental slope. Mar. Geol. 185, 363–377. https://doi.org/10.1016/S0025-3227(01)00298-5

Liu, J.T., Wang, Y.H., Yang, R.J., Hsu, R.T., Kao, S.J., Lin, H.L., Kuo, F.H., 2012. Cyclone-induced hyperpycnal turbidity currents in a submarine canyon. J. Geophys. Res. Ocean. 117, 1–12. https://doi.org/10.1029/2011JC007630

Maier, K.L., Fildani, A., Paull, C.K., Graham, S.A., McHargue, T.R., Caress, D.W., McGann, M., 2011. The elusive character of discontinuous deep-water channels: New insights from Lucia Chica channel system, offshore California. Geology 39, 327–330. https://doi.org/10.1130/G31589.1

Mulder, T., Alexander, J., 2001. Abrupt change in slope causes variation in the deposit thickness of concentrated particle-driven density currents. Mar. Geol. 175, 221–235. https://doi.org/10.1016/S0025-3227(01)00114-1

Mutti, E., 1992. Turbidite sandstones. Agip, Istituto di geologia, Università di Parma.

Mutti, E., Bernoulli, D., Lucchi, F.R., Tinterri, R., 2009. Turbidites and turbidity currents from alpine "flysch" to the exploration of continental margins. Sedimentology 56, 267–318. https://doi.org/10.1111/j.1365-3091.2008.01019.x

Mutti, E., Normark, W.R., 1991. An Integrated Approach to the Study of Turbidite Systems, Springer-Verlag New York. https://doi.org/10.1007/978-1-4684-8276-8_4

Mutti, E., Normark, W.R., 1987. Comparing Examples of Modern and Ancient Turbidite Systems: Problems and Concepts, in: Marine Clastic Sedimentology. Springer Netherlands, Dordrecht, pp. 1–38. https://doi.org/10.1007/978-94-009-3241-8_1

Paull, C.K., Caress, D.W., Ussler, W., Lundsten, E., Meiner-Johnson, M., 2011. High-resolution bathymetry of the axial channels within Monterey and Soquel submarine canyons, offshore central California. Geosphere 7, 1077. https://doi.org/10.1130/GES00636.1

Paull, C.K., Talling, P.J., Maier, K.L., Parsons, D., Xu, J., Caress, D.W., Gwiazda, R., Lundsten, E.M., Anderson, K., Barry, J.P., Chaffey, M., O'Reilly, T., Rosenberger, K.J., Gales, J.A., Kieft, B., McGann, M., Simmons, S.M., McCann, M., Sumner, E.J., Clare, M.A., Cartigny, M.J., 2018. Powerful turbidity currents driven by dense basal layers. Nat. Commun.

Pettingill, H.S., 2004. Global Overview of Deepwater Exploration and Production, in: Weimer, P. (Ed.), Petroleum Systems of Deepwater Settings. Society of Exploration Geophysicists and European Association of Geoscientists and Engineers, pp. 1–40. https://doi.org/10.1190/1.9781560801955.ch2

Prather, B., Booth, J., Steffens, G., Craig, P., 1998. Succession of Seismic Facies of Intraslope Basins , Deep-Water Gulf of Mexico 1. Am. Assoc. Pet. Geol. Bull. 82, 701–728. https://doi.org/10.1306/1D9BC5D9-172D-11D7-8645000102C1865D

Prather, B.E., 2003. Controls on reservoir distribution, architecture and stratigraphic trapping in slope settings. Mar. Pet. Geol. 20, 529–545. https://doi.org/10.1016/j.marpetgeo.2003.03.009

Prather, B.E., 2000. Calibration and visualization of depositional process models for above-grade slopes: A case study from the Gulf of Mexico. Mar. Pet. Geol. 17, 619–638. https://doi.org/10.1016/S0264-8172(00)00015-5

Prather, B.E., O'Byrne, C., Pirmez, C., Sylvester, Z., 2017. Sediment partitioning, continental slopes and base-of-slope systems. Basin Res. 29, 394–416. https://doi.org/10.1111/bre.12190

Prather, B.E., Pirmez, C., Sylvester, Z., Prather, D.S., 2012a. Stratigraphic Response to Evolving Geomorphology in a Submarine Apron Perched on the Upper Niger Delta Slope, in: Prather, B.E., Deptuck, M.E., Mohrig, D., van Hoorn, B., Wynn, R.B. (Eds.), Application of the Principles of Seismic Geomorphology to Continental-Slope and Base-of-Slope Systems: Case Studies from Seafloor and Near-Seafloor Analogues. SEPM (Society for Sedimentary Geology), pp. 145–161.

Prather, B.E., Pirmez, C., Winker, C.D., 2012b. Stratigraphy of Linked Intraslope Basins: Brazos–Trinity System Western Gulf of Mexico, in: Prather, B.E., Deptuck, M.E., Mohrig, D., van Hoorn, B., Wynn, R.B. (Eds.), Application of the Principles of Seismic Geomorphology to Continental-Slope and Base-of-Slope Systems: Case Studies from Seafloor and Near-Seafloor Analogues. SEPM (Society for Sedimentary Geology), pp. 83–109. https://doi.org/10.2110/pec.12.99.0083

Prélat, A., Covault, J.A., Hodgson, D.M., Fildani, A., Flint, S.S., 2010. Intrinsic controls on the range of volumes, morphologies, and dimensions of submarine lobes. Sediment. Geol. 232, 66–76. https://doi.org/10.1016/j.sedgeo.2010.09.010

Ray, F.M., Pinnock, S.J., Katamish, H., Turnbull, J.B., 2010. The Buzzard Field: anatomy of the reservoir from appraisal to production. Pet. Geol. From Matur. Basins to New Front. 7th Pet. Geol. Conf. 369–386. https://doi.org/10.1144/0070369

Sequeiros, O.E., Mosquera, R., Pedocchi, F., 2018. Internal Structure of a Self-Accelerating Turbidity Current. J. Geophys. Res. Ocean. https://doi.org/10.1029/2018JC014061

Shields, A., 1936. Anwendung der Aehnlichkeitsmechanig und der Turbulenzforschung auf die Geschiebebewegung. Mitteilungen der Preußischen Versuchsanstalt für Wasserbau und Schiffbau. Technische Hochschule Berlin.

Smith, D.P., Kvitek, R., Iampietro, P.J., Wong, K., 2007. Twenty-nine months of geomorphic change in upper Monterey Canyon (2002-2005). Mar. Geol. 236, 79–94. https://doi.org/10.1016/j.margeo.2006.09.024

Stacey, C.D., Hill, P.R., Talling, P.J., Enkin, R.J., Hughes Clarke, J., Lintern, D.G., 2018. How turbidity current frequency and character varies down a fjord-delta system: Combining direct monitoring, deposits and seismic data, Sedimentology. https://doi.org/10.1111/sed.12488

Stevenson, C.J., Jackson, C.A.-L., Hodgson, D.M., Hubbard, S.M., Eggenhuisen, J.T., 2015. Deep-Water Sediment Bypass. J. Sediment. Res. 85, 1058–1081. https://doi.org/10.2110/jsr.2015.63

Talling, P.J., Allin, J., Armitage, D. a, Arnott, R.W., Cartigny, M.J., Clare, M. a, Felletti, F., Covault, J. a, Girardclos, S., Hansen, E., Hill, P.R., Hiscott, R.N., Hogg, A.J., Hughes Clarke, J., Jobe, Z.R., Malgesini, G., Mozzato, A., 2015. Key Future Directions for Research on Turbidity Currents and Their Deposits. J. Sediment. Res. 85, 153–169. https://doi.org/10.2110/jsr.2015.03

Talling, P.J., Masson, D.G., Sumner, E.J., Malgesini, G., 2012. Subaqueous sediment density flows: Depositional processes and deposit types. Sedimentology 59, 1937–2003. https://doi.org/10.1111/j.1365-3091.2012.01353.x

Talling, P.J., Wynn, R.B., Masson, D.G., Frenz, M., Cronin, B.T., Schiebel, R., Akhmetzhanov, A.M., Dallmeier-Tiessen, S., Benetti, S., Weaver, P.P.E., Georgiopoulou, A., Zühlsdorff, C., Amy, L.A., 2007. Onset of submarine debris flow deposition far from original giant landslide. Nature 450, 541–544. https://doi.org/10.1038/nature06313

Weimer, P., Slatt, R., 2004. Hybrid-type Deepwater Reservoirs and Pitfalls in the Interpretation of Deepwater Sandstones, in: Petroleum Systems of Deepwater Settings. Society of Exploration Geophysicists and European Association of Geoscientists and Engineers, pp. 1–22. https://doi.org/10.1190/1.9781560801955.ch8

Winker, C.D., 1996. High-Resolution Seismic Stratigraphy of a Late Pleistocene Submarine Fan Ponded by Salt-Withdrawal Mini-Basins on the Gulf of Mexico Continental Slope, in: Offshore Technology Conference. Offshore Technology Conference, pp. 619–628. https://doi.org/10.4043/8024-MS

Wynn, R.B., Kenyon, N.H., Masson, D.G., Stow, D.A.V., Weaver, P.P.E., 2002. Characterization and recognition of deep-water channel-lobe transition zones. Am. Assoc. Pet. Geol. Bull. 86, 1441–1462. https://doi.org/10.1306/61eedcc4-173e-11d7-8645000102c1865d

Wynn, R.B., Masson, D.G., Stow, D.A.V., Weaver, P.P.E., 2000. The Northwest African slope apron: A modern analogue for deep-water systems with complex seafloor topography. Mar. Pet. Geol. 17, 253–265. https://doi.org/10.1016/S0264-8172(99)00014-8

Xu, J.P., 2010. Normalized velocity profiles of field-measured turbidity currents. Geology 38, 563–566. https://doi.org/10.1130/G30582.1

Xu, J.P., Noble, M.A., Rosenfeld, L.K., 2004. In-situ measurements of velocity structure within turbidity currents. Geophys. Res. Lett. 31. https://doi.org/10.1029/2004GL019718

Xu, J.P., Sequeiros, O.E., Noble, M.A., 2014. Sediment concentrations, flow conditions, and downstream evolution of two turbidity currents, Monterey Canyon, USA. Deep. Res. Part I Oceanogr. Res. Pap. 89, 11–34. https://doi.org/10.1016/j.dsr.2014.04.001

Xu, J.P., Swarzenski, P.W., Noble, M., Li, A.C., 2010. Event-driven sediment flux in Hueneme and Mugu submarine canyons, southern California. Mar. Geol. 269, 74–88. https://doi.org/10.1016/j.margeo.2009.12.007

Zhang, Y., Liu, Z., Zhao, Y., Colin, C., Zhang, X., Wang, M., Zhao, S., Kneller, B., 2018. Long-term in situ observations on typhoon-triggered turbidity currents in the deep sea. Geology 3–6.

Zou, C., Zhai, G., Zhang, G., Wang, H., Zhang, G., Li, J., Wang, Z., Wen, Z., Ma, F., Liang, Y., Yang, Z., Li, X., Liang, K., 2015. Formation, distribution, potential and prediction of global conventional and unconventional hydrocarbon resources. Pet. Explor. Dev. 42, 14–28. https://doi.org/10.1016/S1876-3804(15)60002-7

Supplementary material for

The influence of a slope break on turbidite deposits: an experimental investigation

Pohl, F.[a]*, Eggenhuisen, J.T.[a], Cartigny, M.J.B.[b], Tilston, M.[a], de Leeuw, J.[a], Hermidas, N.[c]

[a] Faculty of Geosciences, Utrecht University, P.O. box 80021, 3508 TA Utrecht, The Netherlands
[b] Departments of Geography, Durham University, Lower Mountjoy South Road, DH1 3LE Durham, UK
[c] Faculty of Civil Engineering and Geosciences, TU Delft, P.O. box 5048, 2600 GA Delft, The Netherlands

* Corresponding author: florian.pohl63@gmail.com

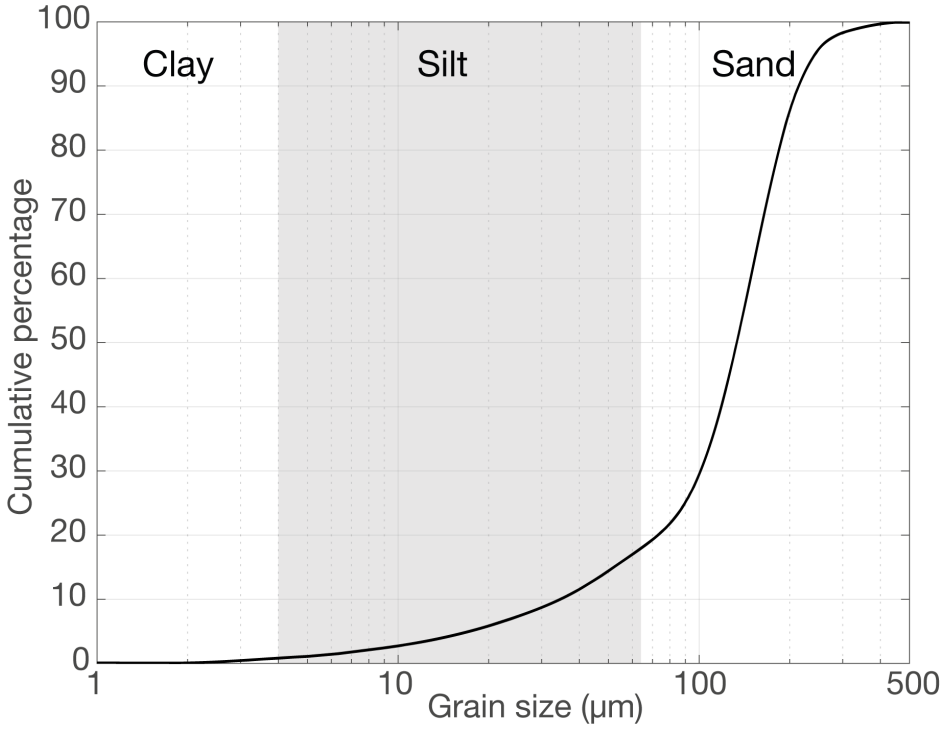

Fig. S1: Grain-size distribution of the sediment which was used for the turbidity current as well as glued to the flume tank floor. The grain-size distribution was measured with a laser particle sizer (Malvern Mastersizer 2000).

Manufacturer and type	MET-FLOW; DUO MX
Speed of sound in water (m/s)	1480
Measurement window (mm)	175.38
Number of channels	238
Distance between channel centres (mm)	0.74
Channel width (mm)	3.7
Frequency of the ultrasound beam (MHz)	1
Number of cycles per pulse	5
Number of sound pulses per measurement	32
Minimum on-axis velocity (mm/s)	-1516.4
Maximum on-axis velocity (mm/s)	1504.5
On-axis velocity resolution (mm/s)	11.8
Pulse repetition frequency (kHz)	4.1

Tab. S1: UVP data acquisition settings.

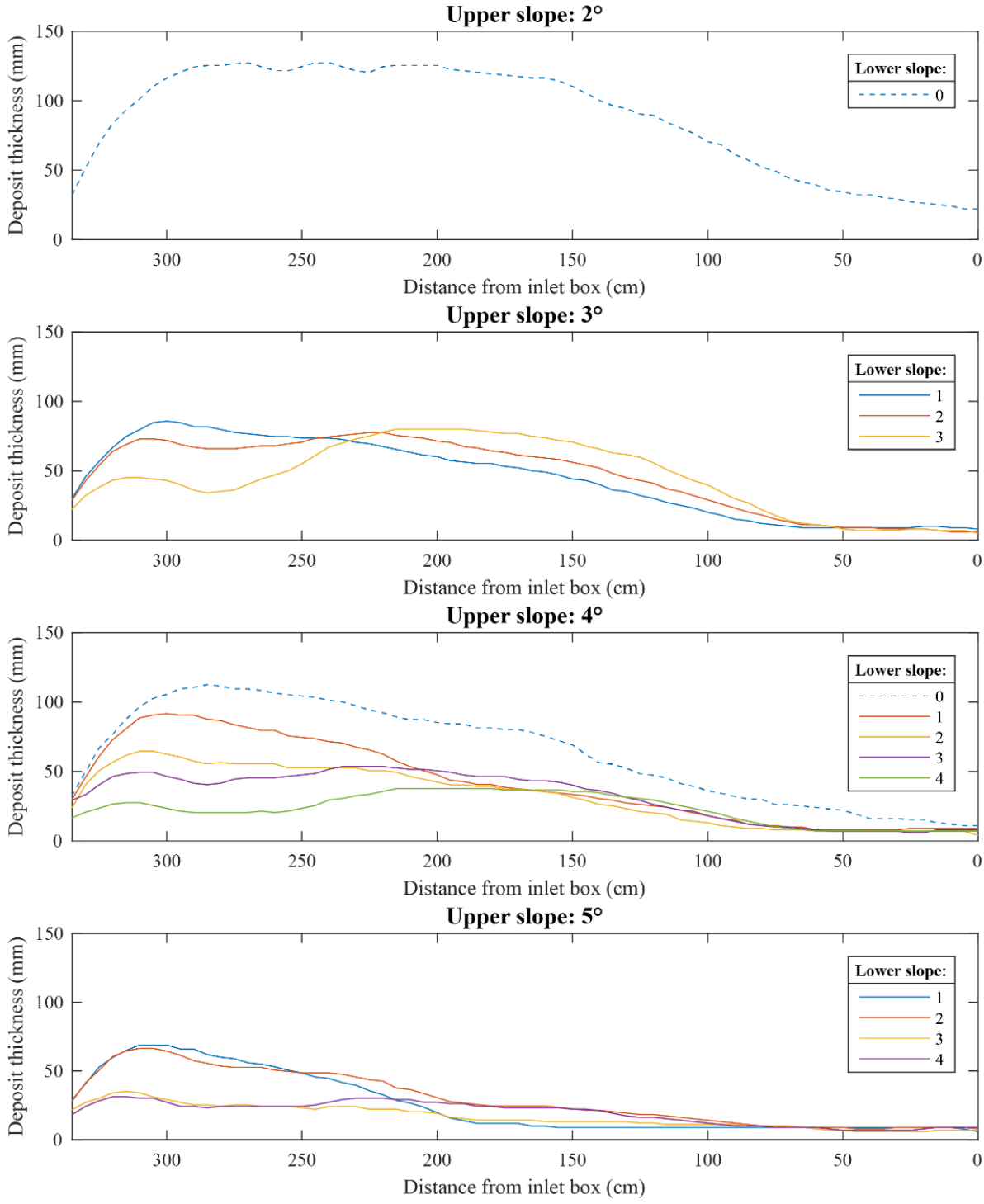

Fig. S2: Deposit profiles of all experiments. The dashed line indicates deposits that were deposited by currents with an exceptional depositional behavior. The dipping angles of the upper and lower slopes are restored to horizontal. The profiles were measured along the length of the flume tank and flow direction was from right to left. The slope break was located 1.7 m downstream from the inlet box.

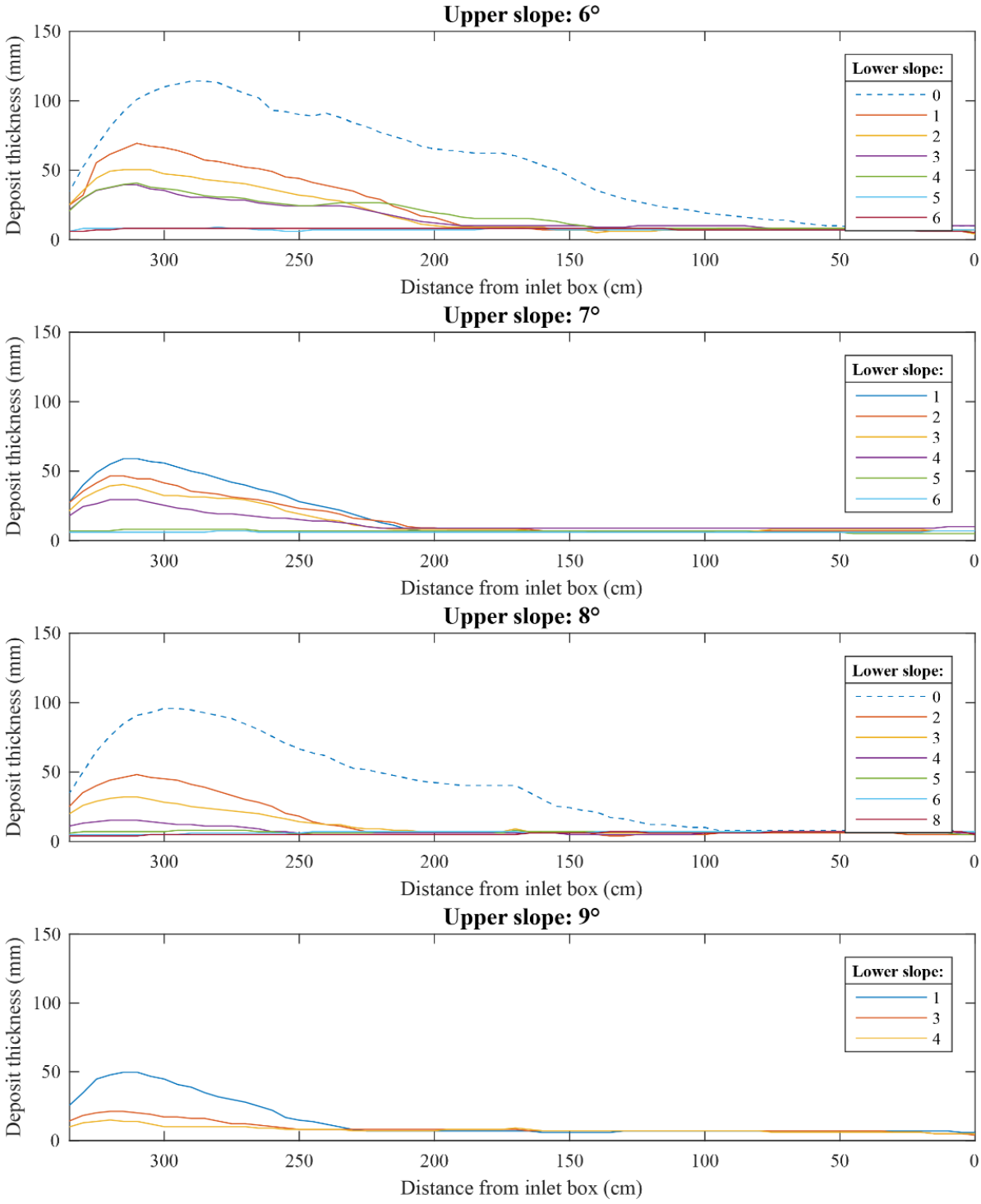

Fig. S2: See caption above.

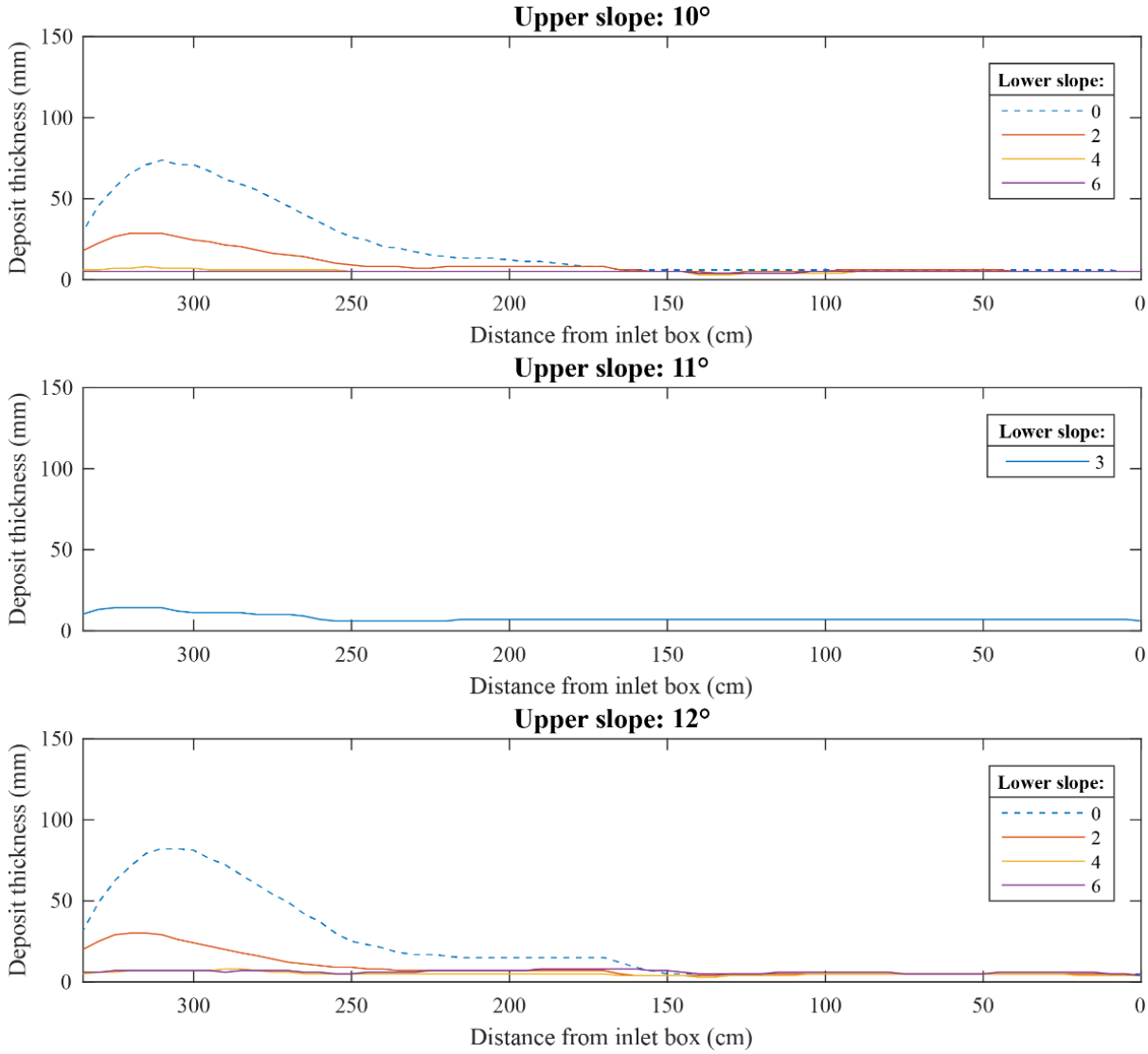

Fig. S2: See caption above.

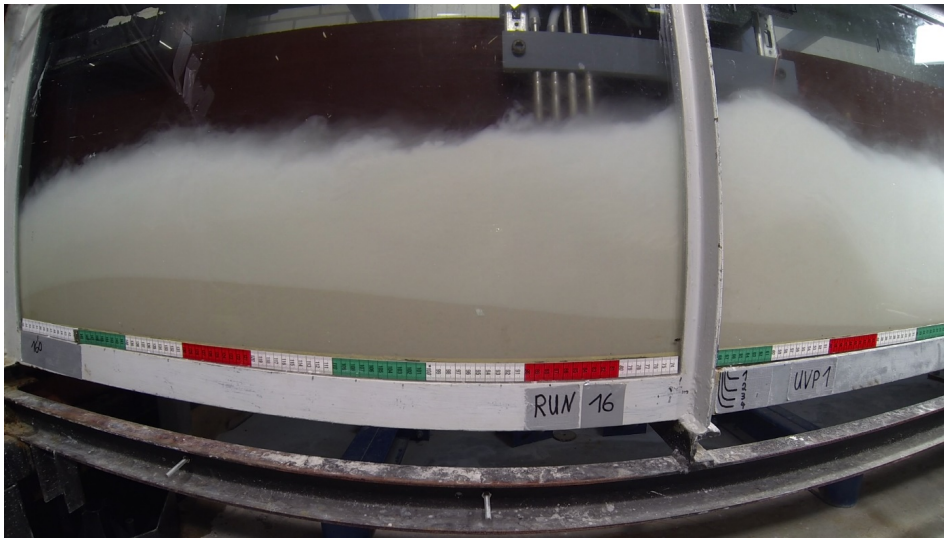

Video S1. Run 07, experiment in which a roller structure developed. In this experiment the upper slope was 8° and the lower slope was 0°. ULR: https://youtu.be/Ny-TN7HMYs0

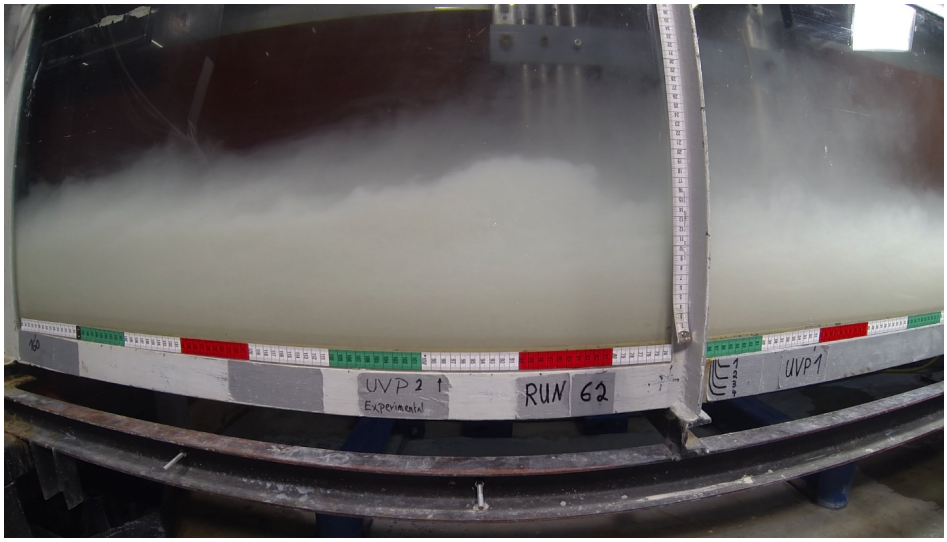

Video S2. Run 41, experiment in which no roller structure. In this experiment the upper slope was 6° and the lower slope was 1°. ULR: https://youtu.be/PMCtaZyj0Ts